Prifysgol Cymru
Y Drindod Dewi Sant
University of Wales
Trinity Saint David

ASSIGNMENT TITLE:

DESIGN & ANALYSIS OF EXTENDED SURFACES

APRIL 7TH 2025

MODULE:ADVANCED THERMOFLUID MECHANICS

MODULE CODE: ACMA6011

Prepared By:

Jordan Briskham

Student Number- 1504704

Contact details- 1504704@student.uwtsd.ac.uk

WORD COUNT: 2710

Abstract

This report examines the historical evolution, modern applications, and thermal optimisation of extended surfaces, commonly referred to as fins, which are crucial in enhancing heat transfer performance across various engineering systems. Initially exploring fins in automotive applications, the report traces their development from early 20th-century water-cooled and air-cooled designs to sophisticated contemporary implementations utilising aluminium, louvred fins, and advanced simulation tools. It further examines fin applications in microprocessor cooling, detailing advancements from passive cooling solutions to advanced materials, such as graphite and graphene, and innovative designs, including heat pipes and additive-manufactured lattice structures.

The analysis encompasses both theoretical and practical evaluations of fins, including temperature distribution, heat transfer optimisation, and material effectiveness. Computational techniques confirm theoretical predictions regarding optimal fin dimensions, emphasising the diminishing returns associated with extended lengths beyond optimal criteria. Comparative assessments of aluminium alloy, brass, copper, and stainless steel rods under controlled conditions validate theoretical expectations, highlighting copper and aluminium as superior conductors due to their thermal properties.

Contents

Introduction 1
1. Historical development and modern application of fins 2
1.1 Development of fins in automotive applications 2
1.1.1 Early 20th Century developments 2
1.1.2 Mid-20th Century Developments 5
1.1.3 Late 20th Century development 7
1.1.4 21st Century development 9
1.2 Development of fins in microprocessor applications 11
1.2.1 Early microprocessor development late 20th Century 11
1.2.2 Further microprocessor development 21st Century 12
1.2.3 Latest advances in fin development 14
2. Plotting the Heat transfer for a fin with an adiabatic tip with the heat transfer rate for an infinitely long fin 18
3. Practical Analysis of Extended Surfaces for Varying Materials 18
3.1 Methodology and calculations 19
3.1.1 Calculating the temperature distribution of an adiabatic tip fin 19
3.1.2 Calculating Perimeter of the fins 20
3.1.3 Calculating cross sectional area of fins 20
3.1.4Calculating the rate of heat transfer of an adiabatic tip fin 21
3.1.5 Calculating m values for rods 21
3.1.6 mL values calculated using original values 22
3.1.7 Temperature distribution plot for 0.4m rods 23
3.1.8 Calculation of heat transfer for each material 24
3.1.9 Data Analysis of the 0.4m Rods 24
3.2 Optimum Length Determination 25
3.2.1 Calculation of Optimum Fin Length 25
3.2.2 Recalculated mL using optimum lengths 26
3.2.3 Heat Loss calculation using optimum lengths 26
3.2.4 Temperature Distribution Plots for Optimum Lengths 27
3.2.5 Analysis of Temperature Distribution for Optimum Lengths 28
3.3 Accurate Fin Length Prediction 28
3.3.1 Solving exponential equation for L 28
3.3.2 Calculating more accurate fin length 29
3.3.3 Recalculated mL using stricter convergence criteria lengths 29

3.3.4Temperature Distribution Plot adjusted for stricter convergence criteria 30
3.3.5 Heat transfer recalculation for stricter convergence criteria 31
3.3.6 Analysis and comparison 32
References 33
Appendices 37
Appendix 1 37
Appendix 2 38
Appendix 3 39

Figures list

Figure 1-Maybach honeycomb radiator-Source:('Honeycomb' radiator, 2025) 2
Figure 2-Tube and fin radiator-Source:(Flat Tube and Fin Radiator Cores, 2025) 3
Figure 3-Representation of a top-down radiator- Source:(Gulhame, 2015) 3
Figure 4-BSA Ten V-Twin air cooled engine-Source:(Baker, 2024) 4
Figure 5-Chevrolet Copper cooled M engine-Source:(MCG, 2022) 5
Figure 6-representation of a cross-flow radiator-Source:(Gulhame, 2015) 6
Figure 7-Louvred radiator fins-Source:(Mohamed et al., 2019) 6
Figure 8-1970s engine fan-Source:(1970 - 1972 Camaro Engine Cooling Clutch Fan Blade, 2025) 7
Figure 9-Brazed aluminium radiator-Source:(Shah, 2003) 8
Figure 10-Aluminium intercooler(bottom) and oil cooler(top)-Source:('Litchfield Toyota GR Yaris Intercooler with Engine Oil Cooler | Litchfield Motors'., 2025) 9
Figure 11-CAD drawing of automotive radiator-Source:(Radiator cooling for car | 3D CAD Model Library | GrabCAD, 2025) 9
Figure 12-CFD analysis of an automotive radiator-Source:(ANSYS FLUENT: CFD simulation for 3D radiator - YouTube, 2022) 10
Figure 13-Representation of EV battery cooling radiators-Source:(Do Electric Vehicles Have Radiators? - CHAL, 2024) 10
Figure 14-Intel 4004 the first commercial microprocessor-Source:(Anthony, 2011) 11
Figure 15-Depiction of a passive heat sink-Source:(Cheung, 2020) 12
Figure 16-Fan-assisted heat sink-Source:(Baknor Thermal Management, Heat Sinks, Liquid Cold Plates & More., 2025) 12
Figure 17-Copper core heat sink-Source:(Noda et al., 2005) 13
Figure 18-Heat pipe stacked fin cooler-Source:(Aslan et al., 2018) 13
Figure 19-Skived aluminium fins-Source:(finskiving.com, 2025) 14
Figure 20-Graphite heat sink-Source:(SIGRATHERM, 2025) 15
Figure 21-Graphene-coated heat sink-Source:(Nicol, 2024) 16
Figure 22-Additive manufactured 3D lattice structure heat sink-Source:(Guo et al., 2021) 16
Figure 23-Fluid-filled oscillating heat pipes-Source:(Chen et al., 2023) 17
Figure 24-Optimum mL criteria plot. 18
Figure 25-Plot showing the temperature distribution of 0.4m metal rods. 23
Figure 26-Plot showing the temperature distribution of the optimum length rods. 27
Figure 27-Plot showing the heat distribution of the four metal rods calculated from the stricter criterion. 30

Equation list

Equation 1-Temperature distribution of an adiabatic tip 19
Equation 2- m equation 20
Equation 3-Perimeter of a circle 20
Equation 4-Cross-sectional area of a circle 27
Equation 5-Heat transfer of an adiabatic fin 21
Equation 6-Optimum fin length equation 25
Equation 7-Temperature distribution for an infinite tip fin 28
Equation 8-Stricter convergence criteria. 28

Table list

Table 1- Material properties 19
Table 2-Calculation of the mL values for the 4 rods. 22
Table 3-Temperature distribution at 0.4m 23
Table 4-Recalculated mL using optimum lengths for the four rods. 26
Table 5-Temperature distribution at optimum lengths 27
Table 6-Recalculated mL values using the lengths calculated from stricter convergence criteria. 29
Table 7-Temperature distribution at more accurate length 30

Introduction

Engineering systems rely heavily on effective heat transfer, which is crucial to performance, reliability, and system longevity. Devices such as heat exchangers and heat sinks utilise extended surfaces, commonly referred to as fins, to enhance convective heat dissipation. These fins significantly enhance heat transfer by increasing the available surface area, thereby improving overall system efficiency. The effectiveness of extended surfaces, however, depends on their specific operating conditions, where efficient design and materials are key in maintaining this heat transfer to promote optimal operation.

This report investigates the design and performance of extended surfaces, emphasising historical and contemporary applications, optimisation techniques, and comparative material performance analyses. Section 1 examines the historical evolution and integration of fins within automotive cooling systems, highlighting notable advancements and extending the analysis to their contemporary utilisation in microprocessor cooling. Section 2 discusses optimising fin dimensions for optimal heat transfer effectiveness. Finally, section 3 presents a detailed thermal analysis of rods composed of four distinct materials. The analysis investigates temperature distributions, calculates optimal fin lengths, and assesses heat transfer performance against theoretical predictions.

1. Historical development and modern application of fins

Extended surfaces, commonly referred to as fins, enhance heat transfer by significantly increasing the surface area. This report section reviews the historical evolution of automotive heat sinks and microprocessor cooling, detailing key developments and recent innovations.

1.1 Development of fins in automotive applications

1.1.1 Early 20th Century developments

1.1.1.1 Water cooled

The early 1900s witnessed significant advancements in automotive industry vehicle cooling technology, laying the groundwork for modern radiator technology. Wilhelm Maybach's introduction of the honeycomb radiator represented a pivotal advancement and early application of extended surfaces within automotive applications(Newcomb et al., 1989). The radiator, constructed predominantly from brass and copper square tubing soldered to prevent leakage, substantially improved convective heat transfer by vastly expanding the surface area available for heat exchange. This innovation dramatically enhanced radiator efficiency and reliability, although it was further improved by the addition of fans in subsequent years, increasing turbulent air flow (Hoyt, 1919).

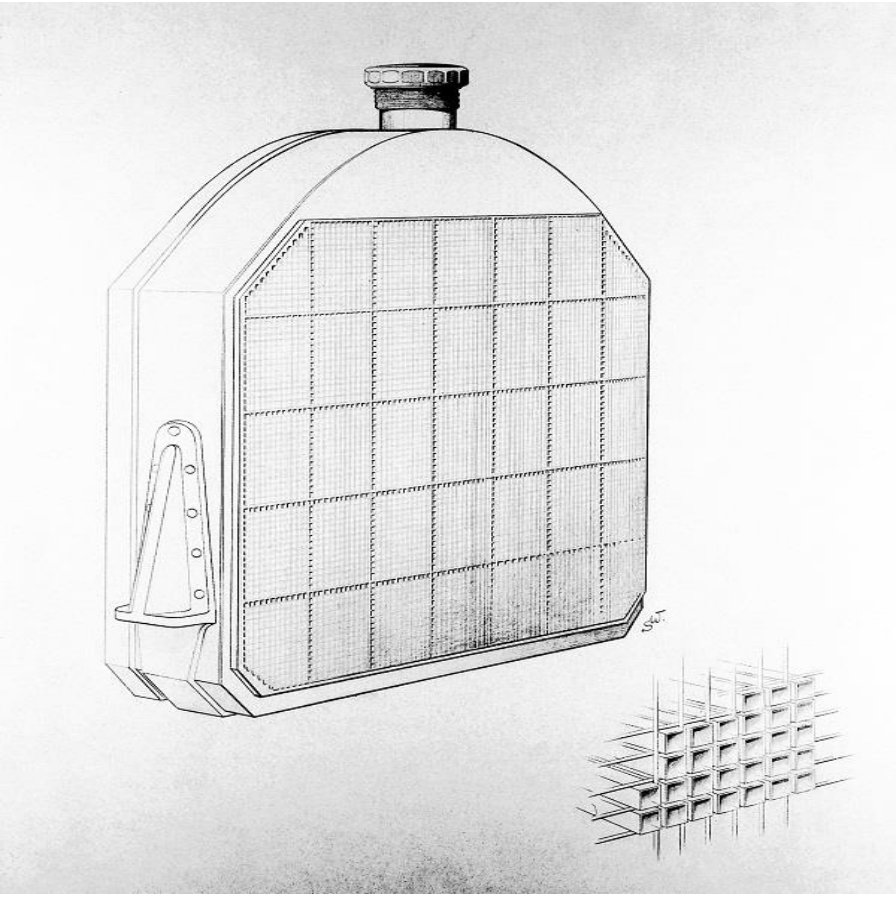

Figure 1-Maybach honeycomb radiator-Source:('Honeycomb' radiator*, 2025)*

By the 1930s and 1940s, automotive manufacturers had refined radiator designs, transitioning toward simpler and more reliable tube-and-fin configurations(Saunders, 1936). These radiators operated on a downflow principle and typically featured vertically aligned tubes combined with horizontal copper fins, striking a balance between efficiency and manufacturing practicality.

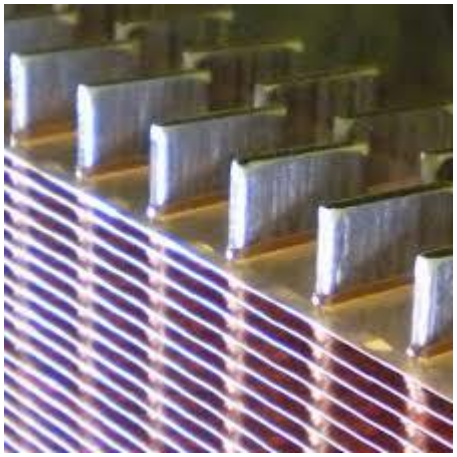

*Figure 2-Tube and fin radiator-Source:(*Flat Tube and Fin Radiator Cores*, 2025)*

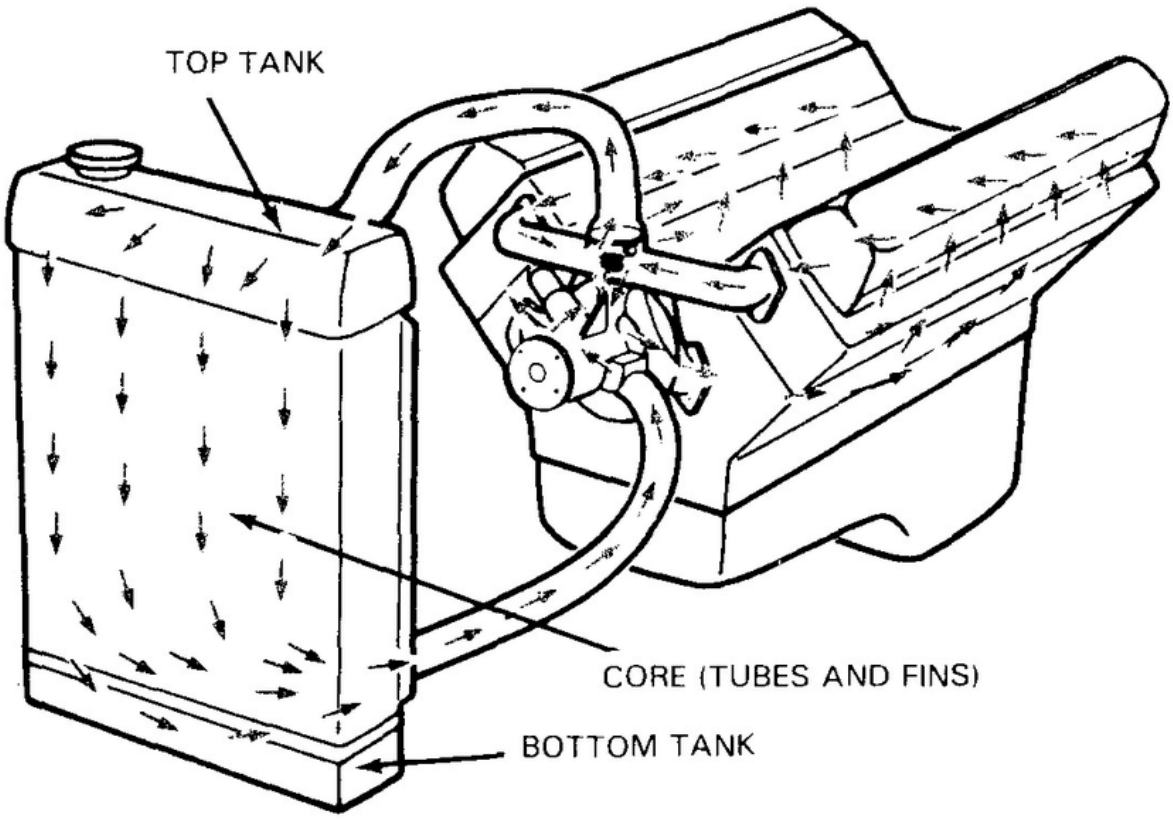

Figure 3-Representation of a top-down radiator- Source:(Gulhame, 2015)

1.1.1.2 Air cooled

The applications of fins in air-cooled combustion engines in motor vehicles have been noted as early as 1884 (Abrams, 2012). Though not as popular as water-cooled engines, these saw parallel development in the early 20th century. Driven by the advancement of aircraft engines post-WWI, research shows that during the 1920s, air-cooled engines were approaching the efficiency of their water-cooled counterparts while remaining more compact due to the need for fewer ancillary parts such as pipes and radiators(Lawrence, 1922). However, these findings are disputed by some who argue that air cooling is far less efficient(Diamant, 1924). Early commercial examples existed from around this time, such as the BSA Ten(Lawrence, 1922), which harnessed cast Iron cylinder heads with deep fins to remove the heat from combustion(Baker, 2024).

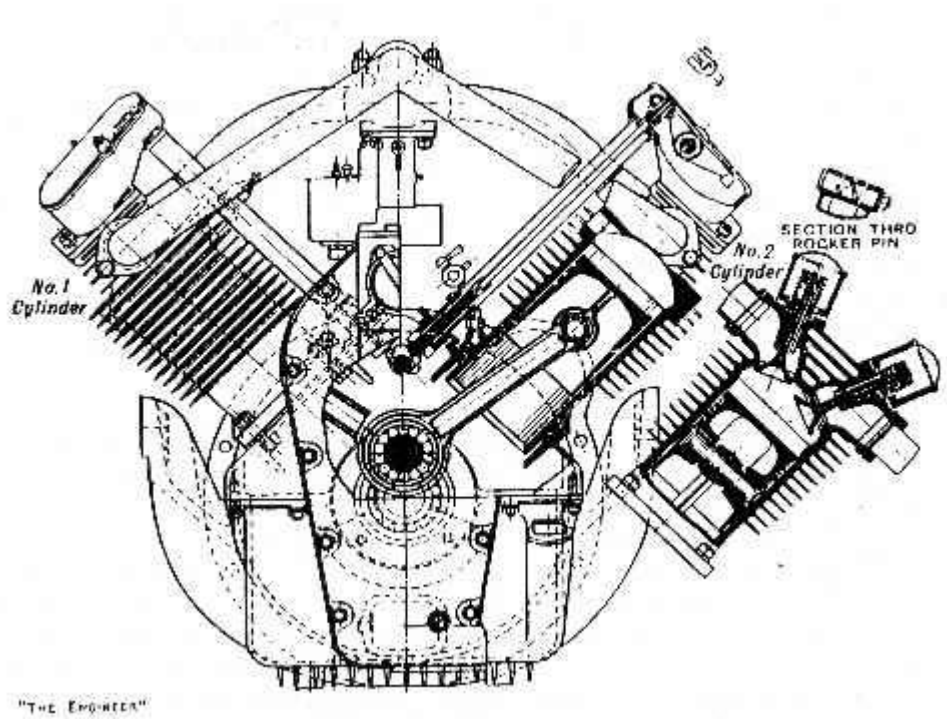

Figure 4-BSA Ten V-Twin air cooled engine-Source:(Baker, 2024)

Further examples include the Copper cooled Chevrolet M. Rather than the traditional cast fin approach, this design incorporated copper plates brazed to cast iron cylinders and used a large fan and shroud to aid in cooling- a feature not present on the BSA(Leslie, 1979). Air-cooled vehicles continued to be developed post-WWII with success, such as the VW beetle(Volkswagen, 2003), but were eventually superseded by water cooling.

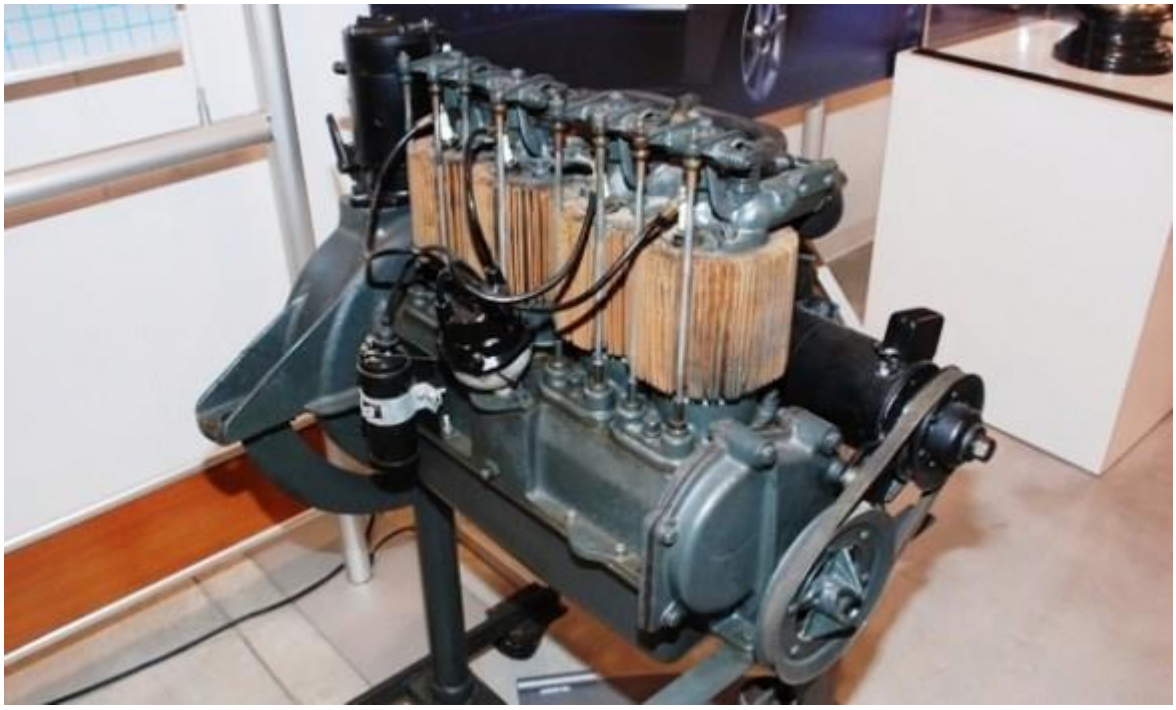

Figure 5-Chevrolet Copper cooled M engine-Source:(MCG, 2022)

1.1.2 Mid-20th Century Developments

The 1950s and 60's witnessed the widespread standardisation of copper-brass radiators within the automotive industry. This era marked a period of increased production efficiency and the introduction of new, more cost-effective radiators, such as tube-to-centre with more robust construction methods improving heat dissipation and radiator durability(Beatenbough, 1968). This period also saw the introduction of innovative radiator architecture, such as the cross-flow radiator design. The crossflow radiator became widely adopted, reflecting manufacturers' increasing emphasis on performance and efficiency.

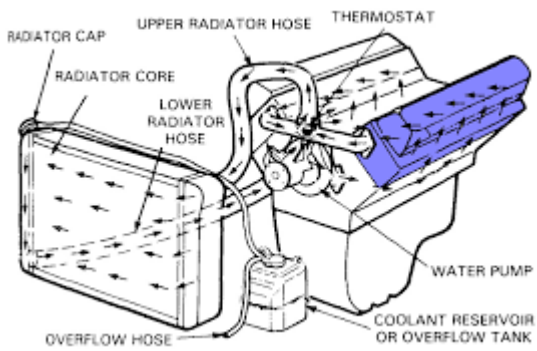

Figure 6-representation of a cross-flow radiator-Source:(Gulhame, 2015)

The oil crises of the 1970s triggered considerable shifts within the automotive sector, compelling manufacturers to prioritise lighter, more fuel-efficient materials, including aluminium(Shariff et al., 2018). Aluminium, despite having lower thermal conductivity compared to copper-brass, offers substantial weight savings, which are critical for improving overall vehicle fuel efficiency. To counteract aluminium's inherently lower heat transfer capabilities, specialised louvred fins were designed(Shah, 2003). The fins create turbulent airflow across the radiator surface. These developments, coupled with advances in cooling fan technology, significantly increase heat dissipation efficiency(Chiou, 1975).

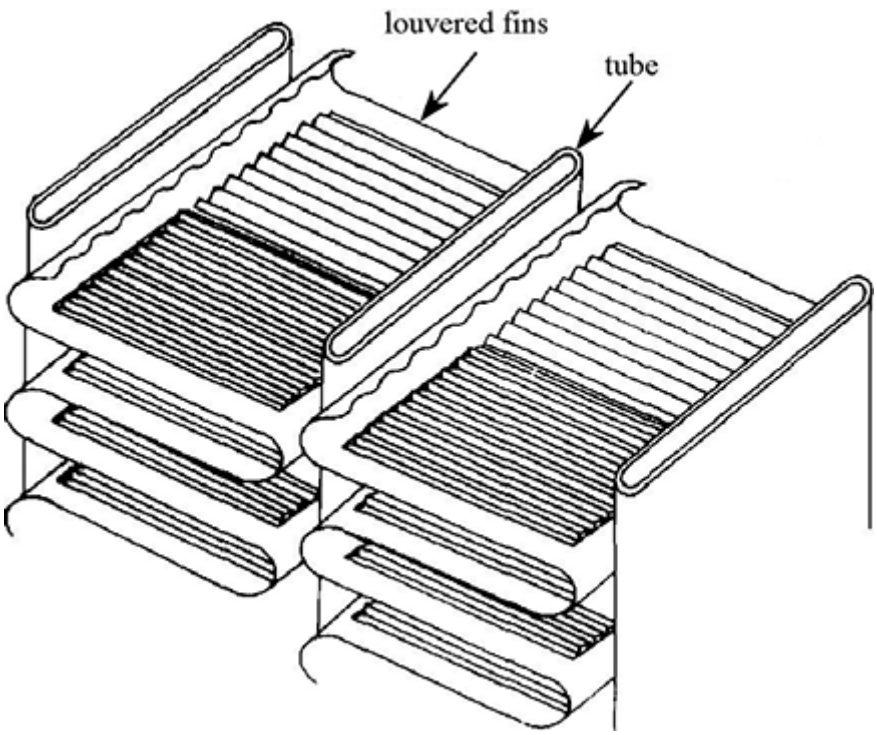

Figure 7-Louvred radiator fins-Source:(Mohamed et al., 2019)

*Figure 8-1970s engine fan-Source:(*1970 - 1972 Camaro Engine Cooling Clutch Fan Blade*, 2025)*

1.1.3 Late 20th Century development

Consequently, by the 1980s, aluminium radiators became firmly established as the industry standard(Fortin et al., 1985). Manufacturers continually improved aluminium radiator designs, introducing vacuum brazed examples which were easier to manufacture, incorporating increased fin densities and multi-row cores, all contributing to enhanced cooling system performance and reliability(Shah, 2003).

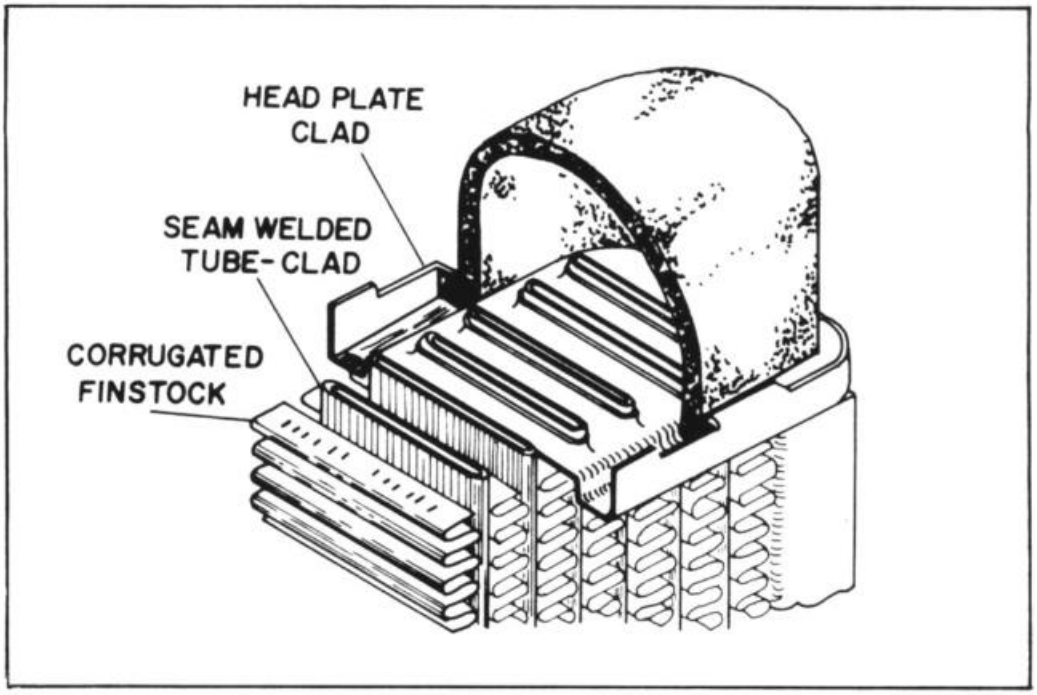

Figure 9-Brazed aluminium radiator-Source:(Shah, 2003)

Throughout the 1990s, vehicle performance improvements and the widespread adoption of technology such as turbochargers saw the need to provide further thermal management solutions, Including Intercoolers and oil coolers(Shibata et al., 1990). Due to an increased presence and limited engine space, more compact radiator solutions were needed, leading to research with computational simulation(Hyun and Pil, 1996).

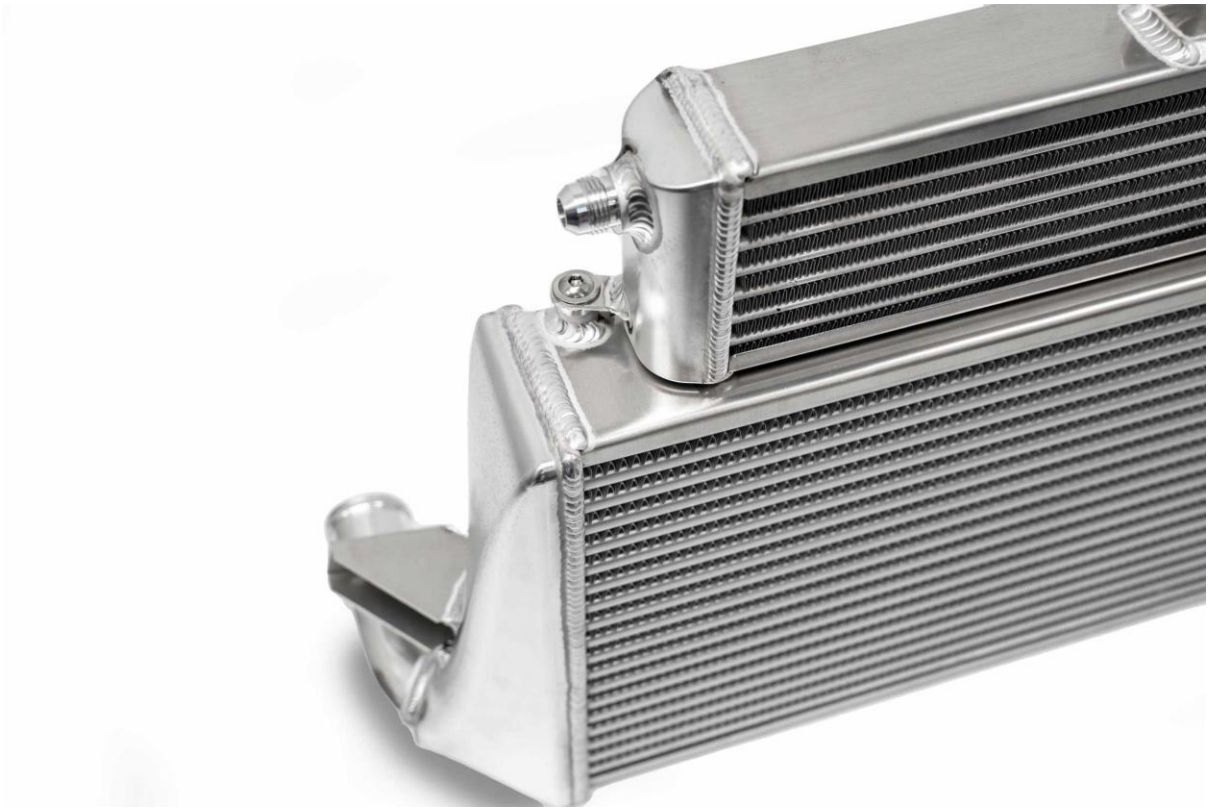

Figure 10-Aluminium intercooler(bottom) and oil cooler(top)-Source:('Litchfield Toyota GR Yaris Intercooler with Engine Oil Cooler | Litchfield Motors'., 2025)

1.1.4 21st Century development

Entering the 2000s, aluminium fins bonded to flat tubes became a standard design approach, greatly facilitated by advancements in computer-aided design (CAD) and Computational Fluid Dynamics (CFD) simulation(Ramesh Kumar et al., 2024). These tools enabled the precise engineering and optimisation of fin geometry, tube arrangements, and airflow dynamics, thereby enhancing radiator performance while reducing production costs(Uhl et al., 2002).

*Figure 11-CAD drawing of automotive radiator-Source:(*Radiator cooling for car | 3D CAD Model Library | GrabCAD*, 2025)*

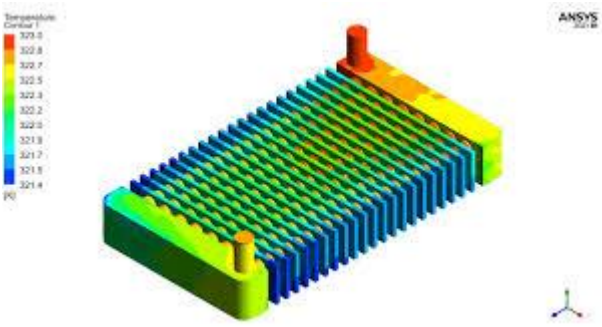

*Figure 12-CFD analysis of an automotive radiator-Source:(*ANSYS FLUENT: CFD simulation for 3D radiator - YouTube*, 2022)*

During this era, automotive cooling solutions expanded significantly to accommodate emerging vehicle technologies, particularly hybrid and electric vehicles (EVs)(Piao et al., 2020). These newer vehicle platforms require unique thermal management solutions beyond traditional engine cooling. Consequently, innovative cooling technologies, such as microchannel cold plates and micro-fin configurations, have been designed explicitly for battery thermal management(Dede, 2014).

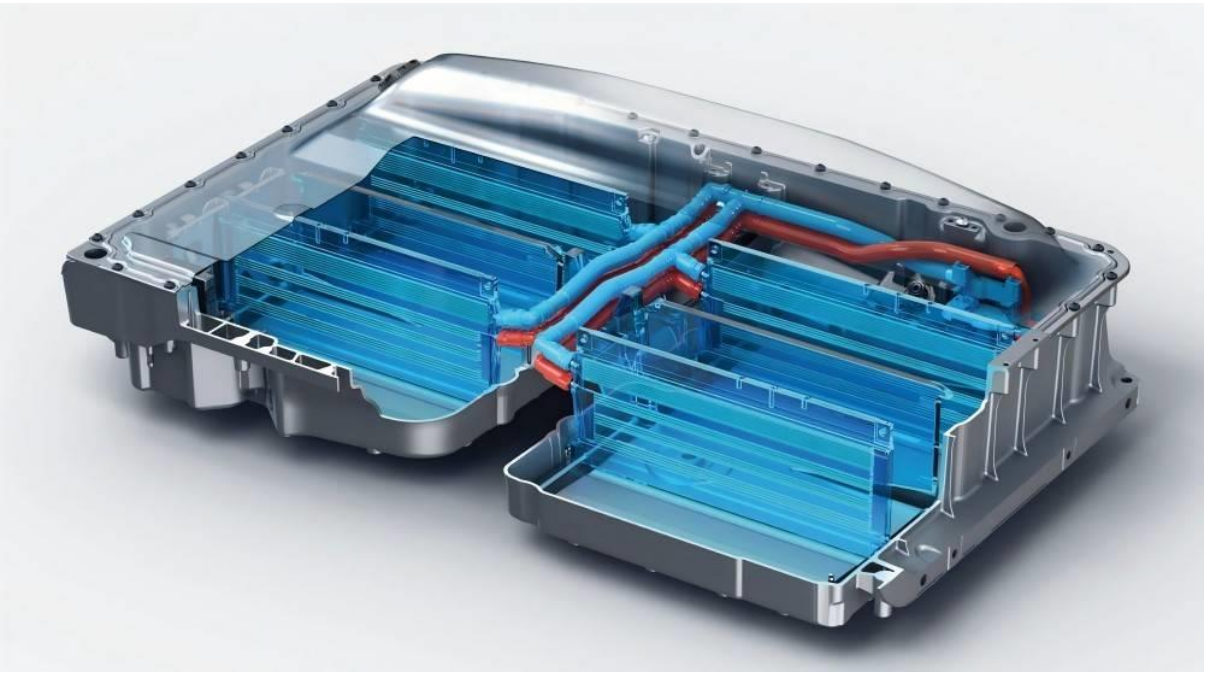

*Figure 13-Representation of EV battery cooling radiators-Source:(*Do Electric Vehicles Have Radiators? - CHAL*, 2024)*

1.2 Development of fins in microprocessor applications

1.2.1 Early microprocessor development late 20th Century

Microprocessor cooling technology has undergone significant developments since its introduction during the 1970s, driven by increasing processor performance and heat generation requirements(Furber, 2017). Initially, Central Processing Units (CPU) required minimal cooling due to their relatively low thermal output(Westcott, 1979), and were passively cooled using their body alone(Hirasawa et al.,2005).

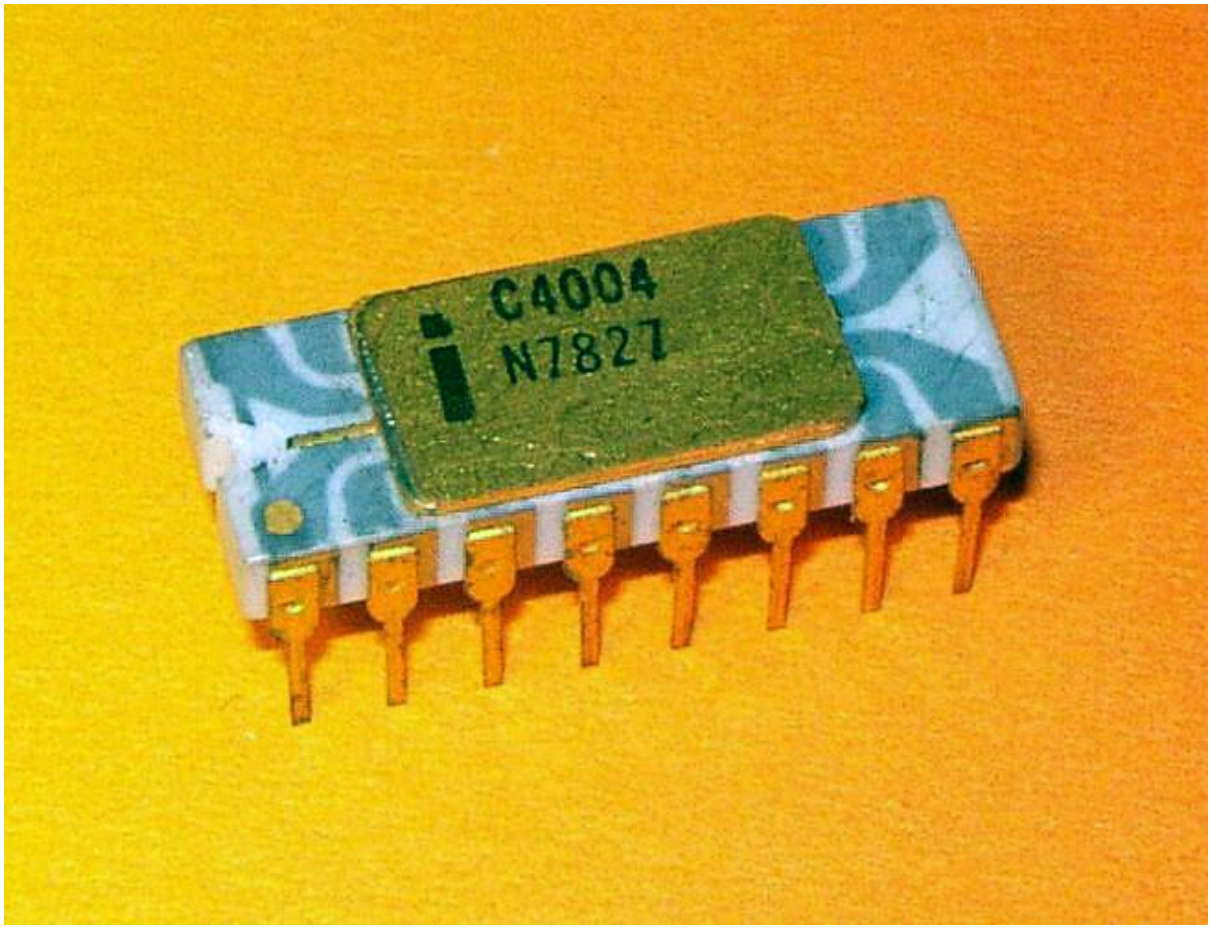

Figure 14-Intel 4004 the first commercial microprocessor-Source:(Anthony, 2011)

However, as microprocessor capabilities expanded dramatically through the 1990s, the heat produced by CPUs increased correspondingly, necessitating more advanced active cooling solutions(Cheung, 2020). Straight-finned heat sinks were employed, made of diecast or extruded aluminium, and occasionally copper if extra cooling performance was required. Initially, these heat sinks relied on ambient air flow (Fig. 14), but as computational power increased, forced convection fans became standard (Fig. 15), significantly improving cooling efficiency. Additionally, integrated

heat spreaders were introduced to distribute heat evenly across the fins, enhancing overall thermal management(Katsutani et al., 2016).

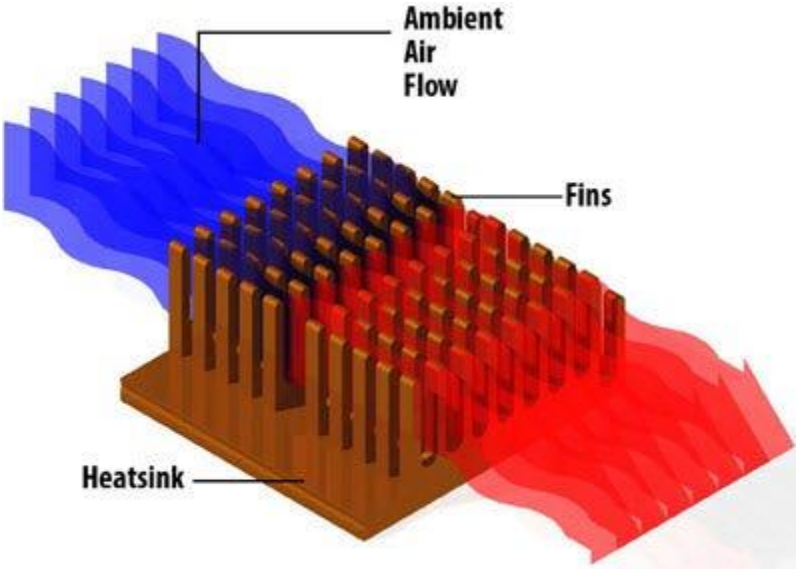

Figure 15-Depiction of a passive heat sink-Source:(Cheung, 2020)

*Figure 16-Fan-assisted heat sink-Source:(*Baknor Thermal Management, Heat Sinks, Liquid Cold Plates & More.*, 2025)*

1.2.2 Further microprocessor development 21st Century

In the early 2000s, technological advancements continued with the introduction of copper cores embedded within aluminium fins, offering superior thermal conductivity and improved efficiency(Noda et al., 2005). Concurrently, heat pipes emerged as a critical innovation, effectively transferring heat from processors to fin arrays(Hirasawa et al., 2005). Furthermore, heat sink designs diversified into pin-fin and radial-fin configurations, which maximised the available surface area and enhanced overall cooling performance(Budimir, 2000) .

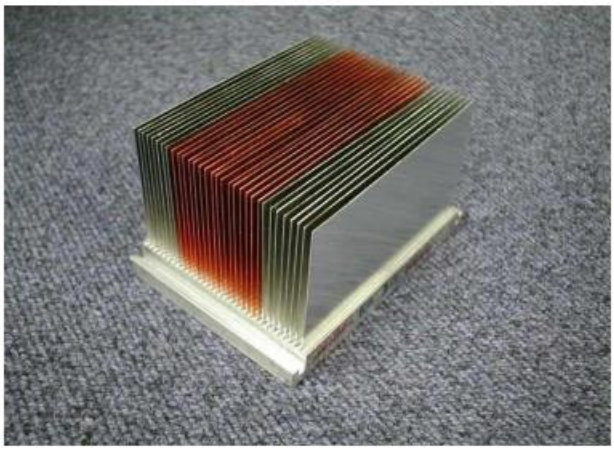

Figure 17-Copper core heat sink-Source:(Noda et al., 2005)

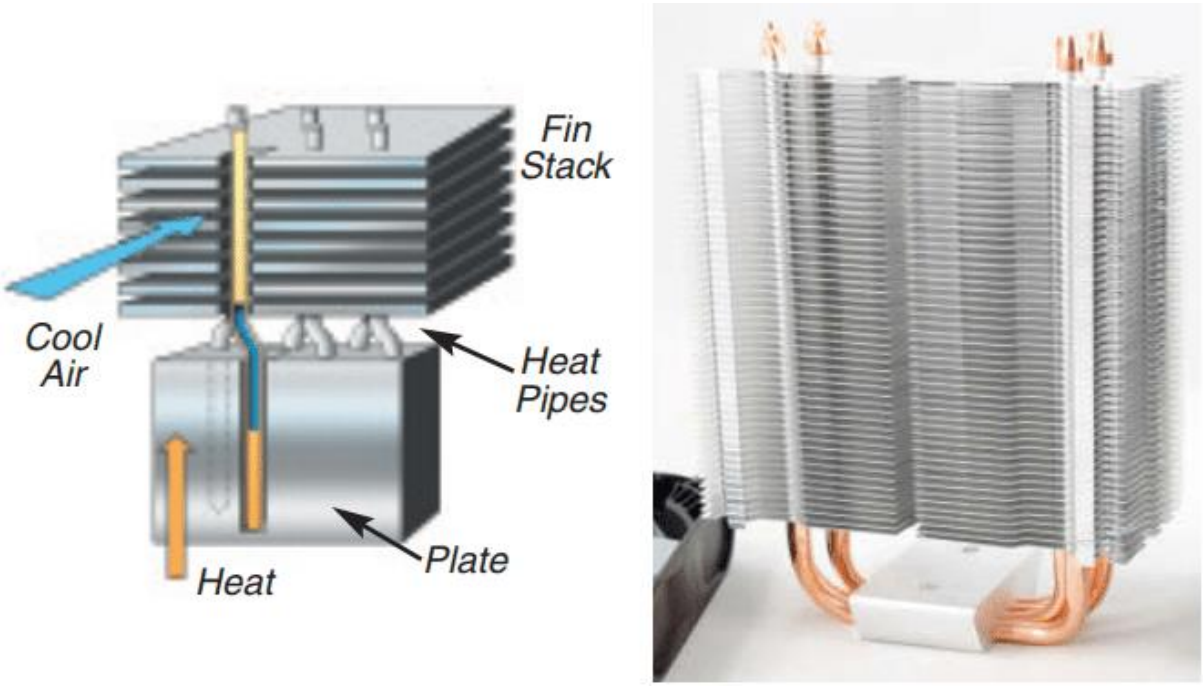

Figure 18-Heat pipe stacked fin cooler-Source:(Aslan et al., 2018)

The 2010s brought further innovations in microprocessor cooling technology. Advances in manufacturing processes, such as skiving and bonding, facilitated thinner and denser fins, increasing the surface area available for heat dissipation(Mochizuki et al., 2011). Vapor chamber technology was adopted more widely, significantly enhancing heat spreading capabilities(Reyes et al., 2012). Additionally, fins began incorporating nanoscale textures, which significantly improved convective heat transfer(Pongiannan et al., 2019).

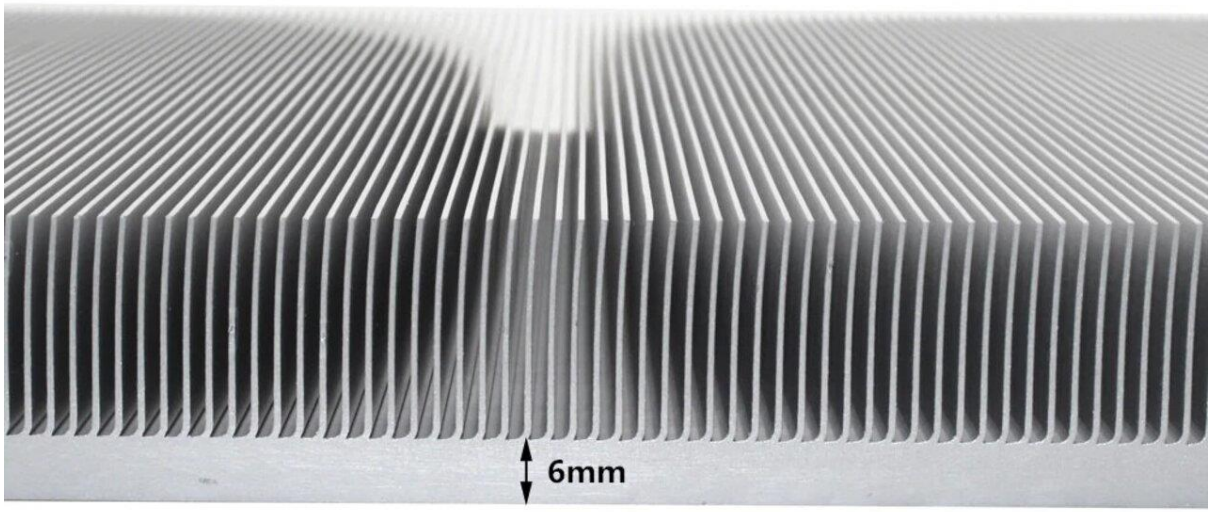

*Figure 19-Skived aluminium fins-Source:(*finskiving.com*, 2025)*

1.2.3 Latest advances in fin development

Recent developments have marked significant progress through the application of advanced materials and manufacturing techniques. Graphite-based fins have emerged as superior alternatives to traditional metals, providing enhanced thermal conductivity alongside substantial weight reductions(Cermak et al., 2017).

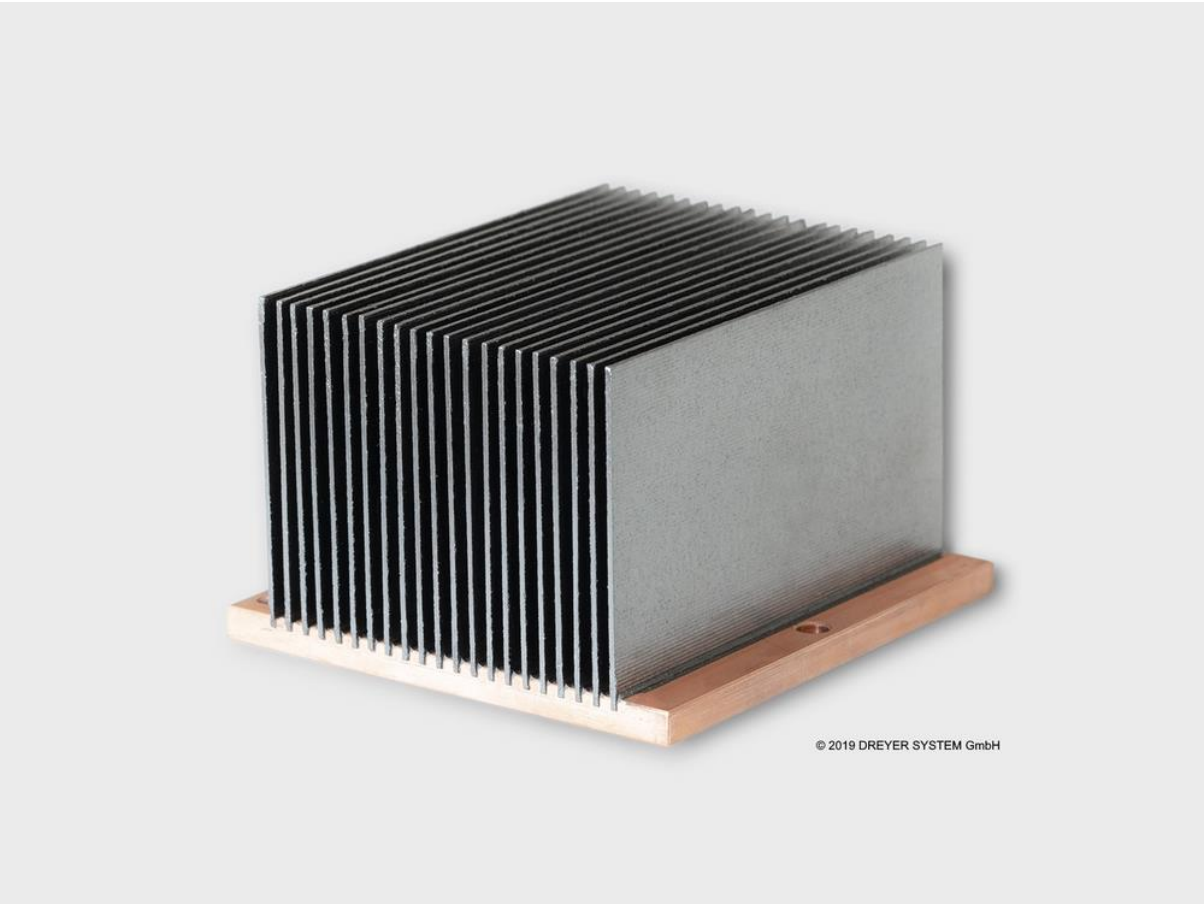

*Figure 20-Graphite heat sink-Source:(*SIGRATHERM*, 2025)*

Graphene coatings have further increased thermal performance(Amirpour et al., 2024). Additionally, nanotechnology has enabled surface enhancements, including carbon nanotube arrays(Farzanehnia et al., 2019), substantially increasing fin surface area and inducing beneficial airflow turbulence, which improves convective heat transfer(Shamsuddin et al., 2021).

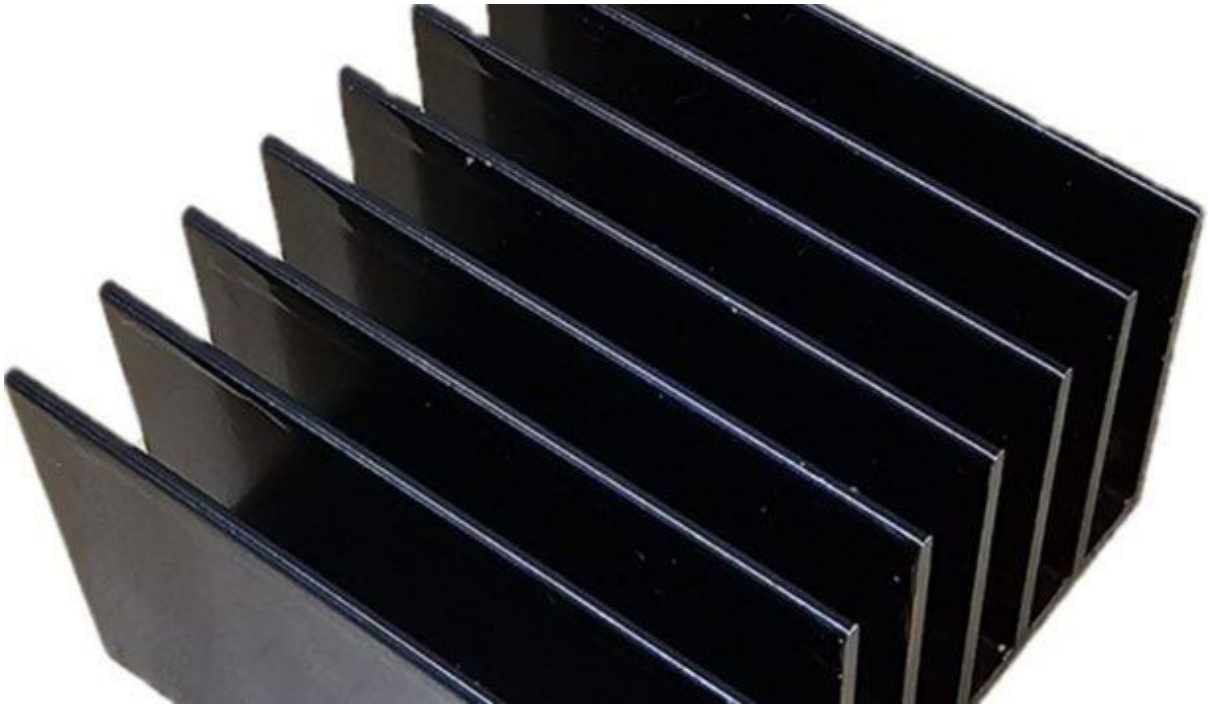

Figure 21-Graphene-coated heat sink-Source:(Nicol, 2024)

Moreover, additive manufacturing (3D printing) technologies have facilitated the creation of complex cooling geometries, such as lattice structures, optimising cooling performance within constrained spaces and enabling multi-material integration(Guo et al., 2021). Fluid-filled and oscillating heat pipes represent another notable innovation, improving heat transport efficiency within compact microprocessor environments(Li et al., 2024).

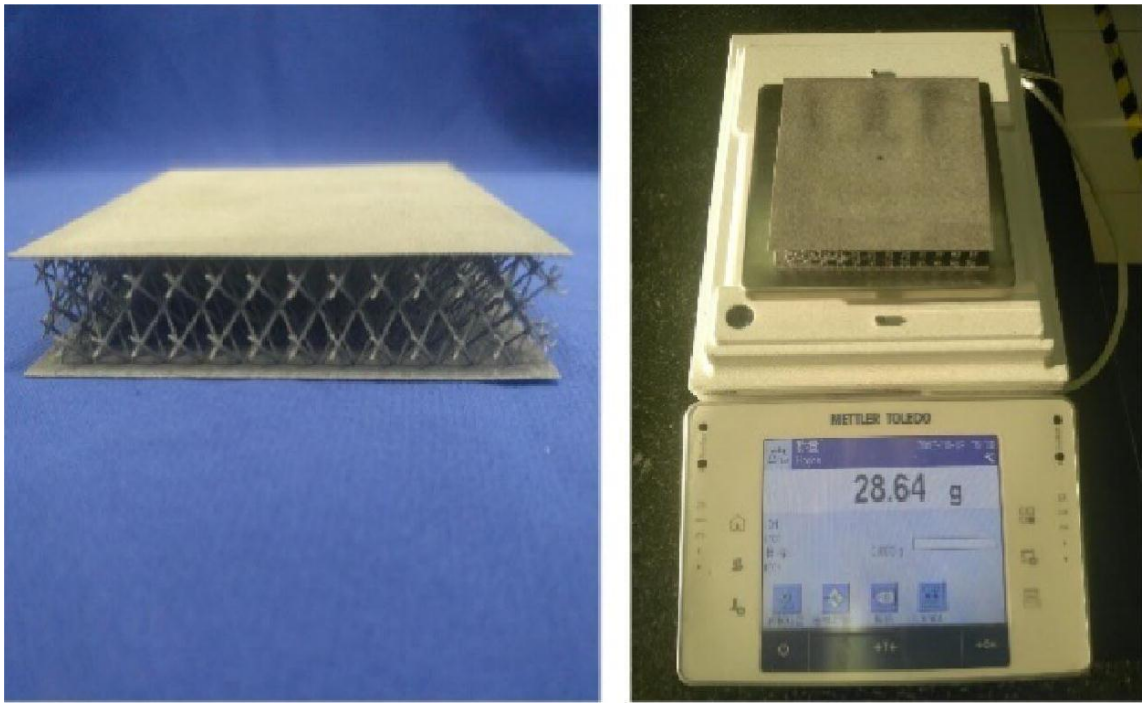

Figure 22-Additive manufactured 3D lattice structure heat sink-Source:(Guo et al., 2021)

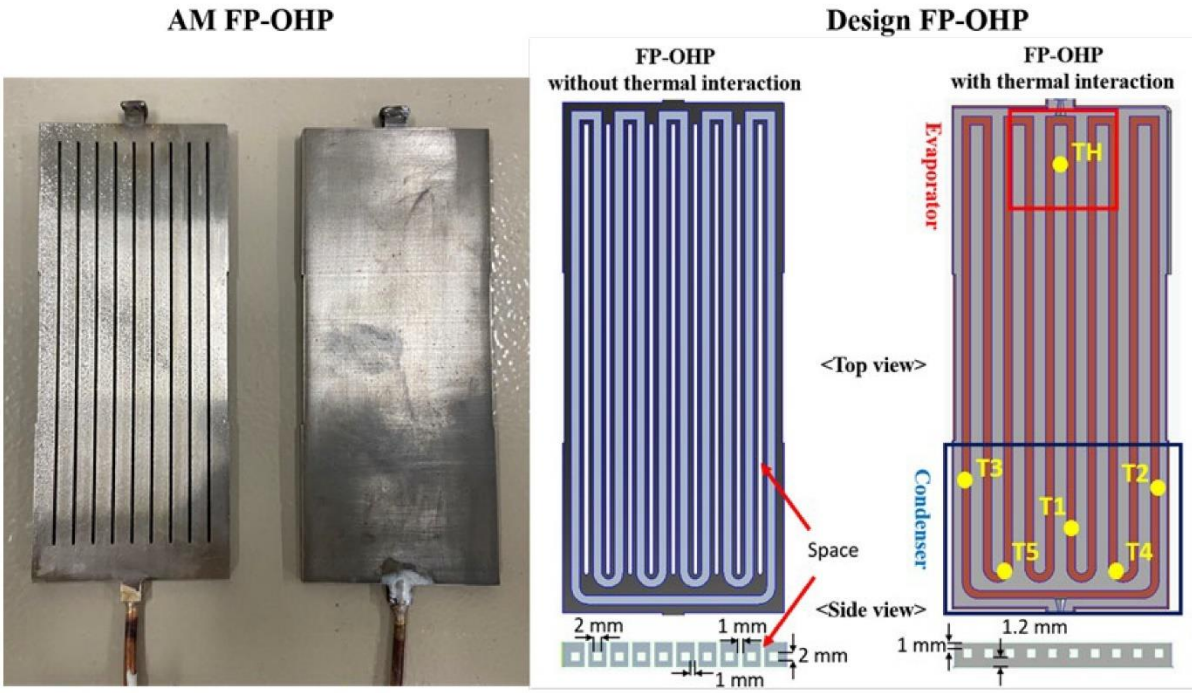

Figure 23-Fluid-filled oscillating heat pipes-Source:(Chen et al., 2023)

These recent advances offer numerous practical advantages. Enhanced thermal performance from advanced materials and design optimisation significantly reduces thermal resistance, thereby enhancing reliability and overall system performance. The adoption of graphite and other lightweight composites significantly reduces component weight(Cermak et al., 2017). Lastly, sustainability and cost efficiency have notably improved through innovations in materials, precision manufacturing, and additive production processes(Guo et al., 2021). These advancements collectively reduce environmental impact, minimise production costs, decrease material wastage, and extend component lifespan, reflecting the broader industrial trend towards sustainable and economically viable technology solutions(Chen et al., 2025).

2. Plotting the Heat transfer for a fin with an adiabatic tip with the heat transfer rate for an infinitely long fin

The heat transfer of a fin was plotted to demonstrate the relationship between the ratio of heat transfer rates for a fin with an adiabatic tip versus that of an infinitely long fin as a function of the parameter mL. The graph was generated using Excel, plotting values of the hyperbolic tangent term of mL from 0 to 4 in increments of 0.1. The resulting plot confirms that the optimal fin length corresponds to an mL value of approximately 2.65, which is consistent with theoretical expectations(Incropera et al., 2007).

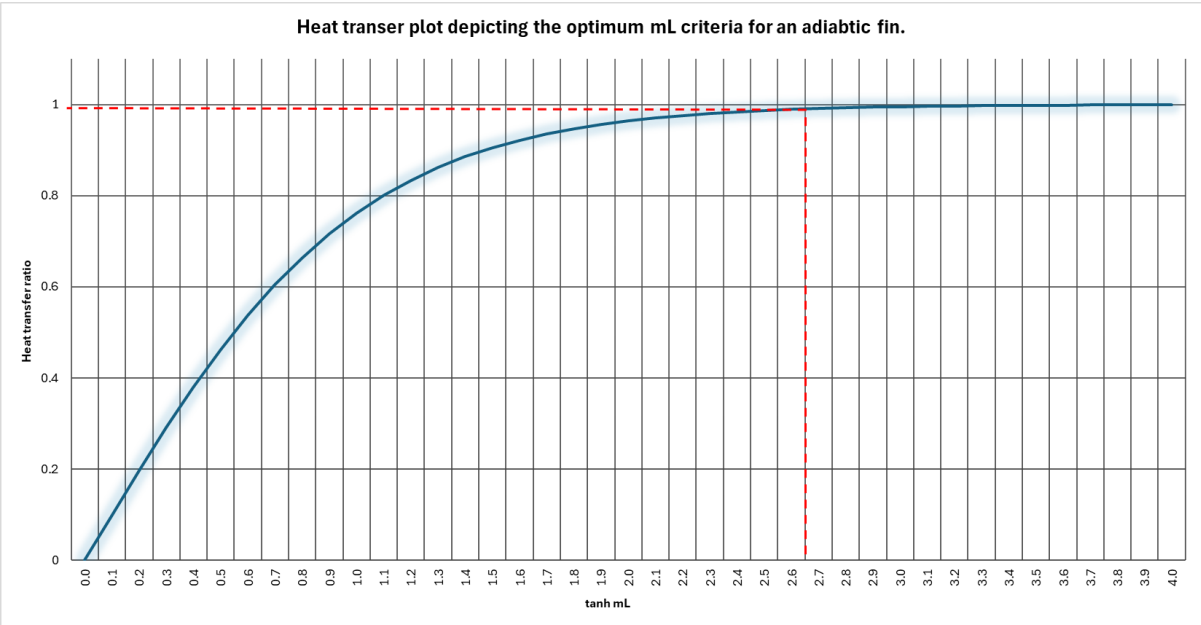

Figure 24-Optimum mL criteria plot.

3. Practical Analysis of Extended Surfaces for Varying Materials

This section examines the temperature distribution and heat loss characteristics of four different rod materials, each exposed to convective heat transfer with ambient air.

A cylindrical rod with a diameter of 7.5 mm is considered, with one end attached to a heated surface at 110°C, while the surrounding air is maintained at 18°C. The objective of this study is to analyse how heat dissipates along the length of the rod and how varying material properties (Tab.1) affect the temperature distribution and heat dissipation.

Material	h(W/m^2 K)	K (W/m K)
2024 Aluminium alloy	30	186
Brass (70 Cu/30 Zn)	30	99
Copper	15	398
304 Stainless Steel	7.5	16

Table 1- Material properties

3.1 Methodology and calculations

3.1.1 Calculating the temperature distribution of an adiabatic tip fin

The temperature variation along the rod length is computed and plotted for a length of 0.4 m, using increments of 10 mm, enabling a direct comparison among the materials. As a finite length parameter is provided in this case, an adiabatic tip boundary condition applies expressed as(Lienhard, 2020):

$$T(x) = T_\infty + (T_b - T_\infty) \cdot \frac{\cosh[m(L-x)]}{\cosh(mL)}$$

Equation 1-Temperature distribution of an adiabatic tip

Where:

$T(x)$ = Temperature at position x Along the fin.

$T_\infty =$ Ambient temperature (temperature of the surrounding fluid).

$T_b =$ Base temperature (temperature at the base of the fin, $x = 0$)

$L =$ Length of the fin.

$x =$ Position along the fin, measured from the base ($x = 0$ is at the base, $x = L$ Is at the tip).

$\cosh =$ Hyperbolic cosine function.

$m =$ A dimensionless parameter that depends on the fin's material properties and heat transfer characteristics and is given by(Lienhard, 2020):

$$m = \sqrt{\frac{hP}{kA_c}}$$

Equation 2- m equation

Where:

$h =$ Convective heat transfer coefficient.

$P =$ Perimeter of the fin.

$k =$ Thermal conductivity of the fin material.

$A_c =$ Cross-sectional area of the fin.

3.1.2 Calculating Perimeter of the fins

Equation 3 shows the formula for calculating the perimeter of the rods(Bird, 2021):

$$P = 2\pi r$$

Equation 3-Perimeter of a circle

$$\therefore$$

$$P = 2 \times \pi \times (3.75 \times 10^{-3})$$

$$P = 2.63 \times 10^{-2}\ m$$

3.1.3 Calculating cross sectional area of fins

Equation 4 shows the formula for calculating the cross-sectional area of the rods(Bird, 2021):

$$A_c = \pi r^2$$

Equation 4-Cross sectional area of a circle

$$\therefore$$

$$A_c = \pi \times (3.75 \times 10^{-3})^2$$

$$A_c = 4.42 \times 10^{-5}\ m^2$$

3.1.4Calculating the rate of heat transfer of an adiabatic tip fin

To determine the heat loss for the four materials, it is necessary to calculate the heat transfer of an adiabatic fin expressed as(Lienhard, 2020):

$$\dot{Q} = \sqrt{hPkA_c}(T_b - T_\infty) \cdot \tanh(\mathrm{mL})$$

Equation 5-Heat transfer of an adiabatic fin

Where:

$\dot{Q}$= Heat transfer rate from the fin.

$\tanh =$ Hyperbolic tangent function.

3.1.5 Calculating m values for rods

The material properties shown in Tab.1 were defined in a Microsoft Excel file to allow for the calculation of the m value, as well as the plotting of the temperature distribution using the formulae given in Section 3.1.1.

3.1.5.1 Aluminium alloy

$$m = \sqrt{\frac{30 \times 0.263}{186 \times 0.0375}}$$

$$m = 9.2748$$

3.1.5.2 Brass

$$m = \sqrt{\frac{30 \times 0.263}{99 \times 0.0375}}$$

$$m = 12.7128$$

3.1.5.3 Copper

$$m = \sqrt{\frac{15 \times 0.263}{398 \times 0.0375}}$$

$$m = 4.4834$$

3.1.5.4 Stainless steel

$$m = \sqrt{\frac{7.5 \times 0.263}{16 \times 0.0375}}$$

$$m = 15.8114$$

3.1.6 mL values calculated using original values

Material	mL	=
2024 Aluminium alloy	9.2748 X 0.4	3.71
Brass (70 Cu/30 Zn)	12.7128 X 0.4	5.09
Copper	4.4834 X 0.4	1.79
304 Stainless Steel	15.8114 X 0.4	6.32

Table 2-Calculation of the mL values for the 4 rods.

3.1.7 Temperature distribution plot for 0.4m rods

The full data range is provided in App.1.

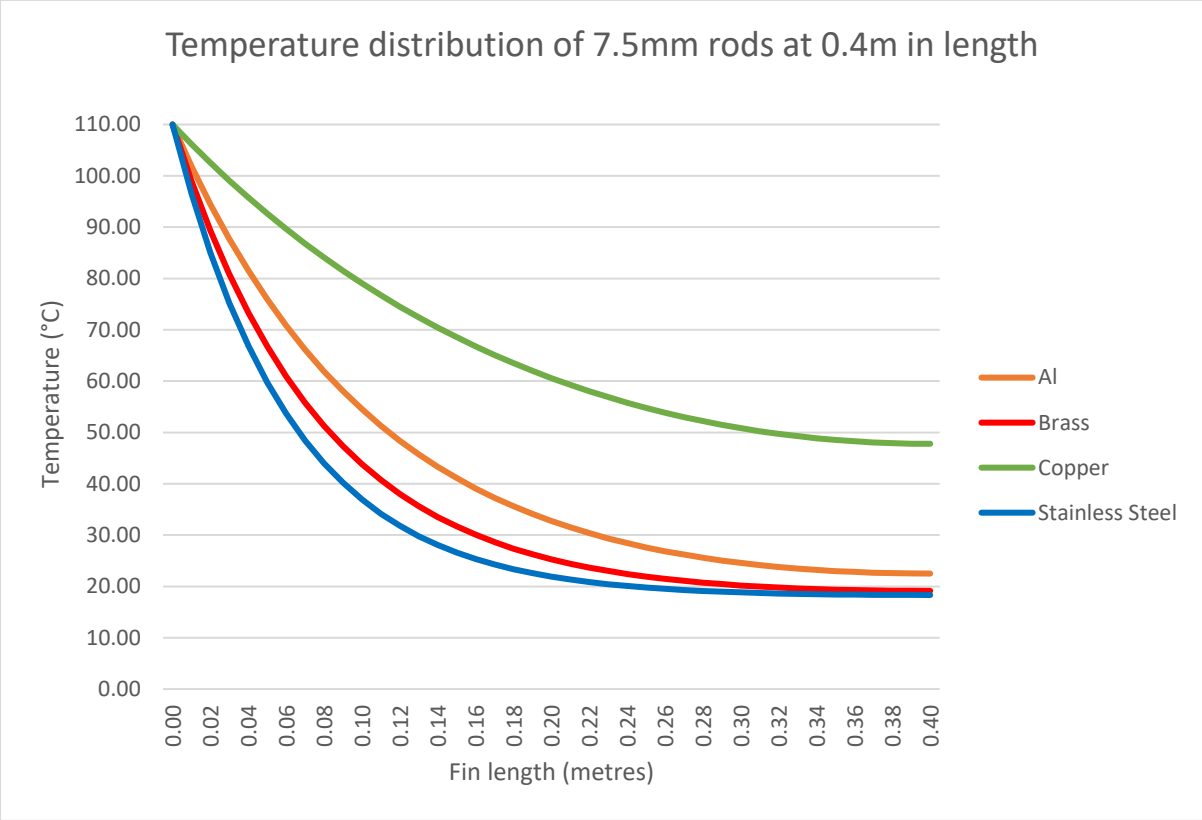

Figure 25-Plot showing the temperature distribution of 0.4m metal rods.

Material	Temperature distribution at 0.4m (°C)
Aluminium	22.50
Brass	19.14
Copper	47.79
Stainless steel	18.33

Table 3-Temperature distribution at 0.4m

3.1.8 Calculation of heat transfer for each material

Using the adiabatic fin approximation expressed in Eq.1 the heat loss for the four 0.4m rods are calculated:

3.1.8.1 Aluminium alloy

$$\dot{Q} = \sqrt{30 \times (0.236) \times 186 \times (0.0375)}(110 - 18) \cdot \tanh(9.2748 \times 0.4)$$

$$\dot{Q} = 7.00\ W$$

3.1.8.2 Brass

$$\dot{Q} = \sqrt{30 \times (0.236) \times 99 \times (0.0375)}(110 - 18) \cdot \tanh(12.7128 \times 0.4)$$

$$\dot{Q} = 5.11\ W$$

3.1.8.3 Copper

$$\dot{Q} = \sqrt{15 \times (0.236) \times 398 \times (0.0375)}(110 - 18) \cdot \tanh(4.483 \times 0.4)$$

$$\dot{Q} = 6.86\ W$$

3.1.8.4 Stainless Steel

$$\dot{Q} = \sqrt{7.5 \times (0.236) \times 16 \times (0.0375)}(110 - 18) \cdot \tanh(9.2748 \times 0.4)$$

$$\dot{Q} = 1.03\ W$$

3.1.9 Data Analysis of the 0.4m Rods

Fig.25 clearly illustrates an exponential decay curve along each rod. Copper and Aluminium rods maintain a higher temperature further from the base(Tab.3) due to their higher thermal conductivity and lower m values compared to brass and stainless steel. This correlates with the results shown here, as both latter materials experience the steepest drop, with stainless steel reaching near-ambient temperature the fastest. This suggests that their lower thermal conductivity results in less effective heat conduction. Furthermore, the plot indicates that the fin length for copper is not at an optimal level, as the temperature has not dropped to a near-ambient temperature (Tab. 3). The adiabatic boundary condition insulates the tip, meaning no heat escapes from the very end of the fin. Therefore, all the heat that enters at the base must exit along the fin's lateral surface by convection. The hyperbolic tangent factor accounts for the fact that longer fins eventually deliver nearly the same heat transfer as a fin with an infinite boundary length, while shorter fins never reach their maximum potential(Incropera et al., 2007).

3.2 Optimum Length Determination

Using the optimum mL parameter expressed in 3.1, an optimum length can be determined using(Incropera et al., 2007):

$$L_{opt} = \frac{2.65}{m}$$

Equation 6-Optimum fin length equation.

Where:

L_{opt} = Optimum length of fin

3.2.1 Calculation of Optimum Fin Length

Using Eq.6, the optimum fin lengths for each material are calculated as:

3.2.1.1 Aluminium alloy

$$L_{opt} = \frac{2.65}{9.2748}$$

$$L_{opt} = 0.2857\ m$$

3.2.1.2 Brass

$$L_{opt} = \frac{2.65}{12.7128}$$

$$L_{opt} = 0.2085\ m$$

3.2.1.3 Copper

$$L_{opt} = \frac{2.65}{4.4834}$$

$$L_{opt} = 0.5911\ m$$

3.2.1.4 Stainless steel

$$L_{opt} = \frac{2.65}{15.8114}$$

$$L_{opt} = 0.1676\ m$$

3.2.2 Recalculated mL using optimum lengths

Material	mL	=
2024 Aluminium alloy	9.2748 X 0.2857	2.65
Brass (70 Cu/30 Zn)	12.7128 X 0.2085	2.65
Copper	4.4834 X 0.5911	2.65
304 Stainless Steel	15.8114 X 0.1676	2.65

Table 4-Recalculated mL using optimum lengths for the four rods.

3.2.3 Heat Loss calculation using optimum lengths

Using the adiabatic fin approximation expressed in Eq.1 the heat loss for the four optimum length rods are calculated:

3.2.3.1 Aluminium alloy

$$\dot{Q} = \sqrt{30 \times (0.236) \times 186 \times (0.0375)} \cdot (110 - 18) \cdot \tanh(9.2748 \times 0.2857)$$

$$\dot{Q} = 6.94\ W$$

3.2.3.2 Brass

$$\dot{Q} = \sqrt{30 \times (0.236) \times 99 \times (0.0375)} \cdot (110 - 18) \cdot \tanh(12.7128 \times 0.2085)$$

$$\dot{Q} = 5.06\ W$$

3.2.3.3 Copper

$$\dot{Q} = \sqrt{15 \times (0.236) \times 398 \times (0.0375)} \cdot (110 - 18) \cdot \tanh(4.483 \times 0.5911)$$

$$\dot{Q} = 7.18\ W$$

3.2.3.4 Stainless Steel

$$\dot{Q} = \sqrt{7.5 \times (0.236) \times 16 \times (0.0375)} \cdot (110 - 18) \cdot \tanh(9.2748 \times 0.1676)$$

$$\dot{Q} = 1.02\ W$$

3.2.4 Temperature Distribution Plots for Optimum Lengths

The full data range is provided in App.2.

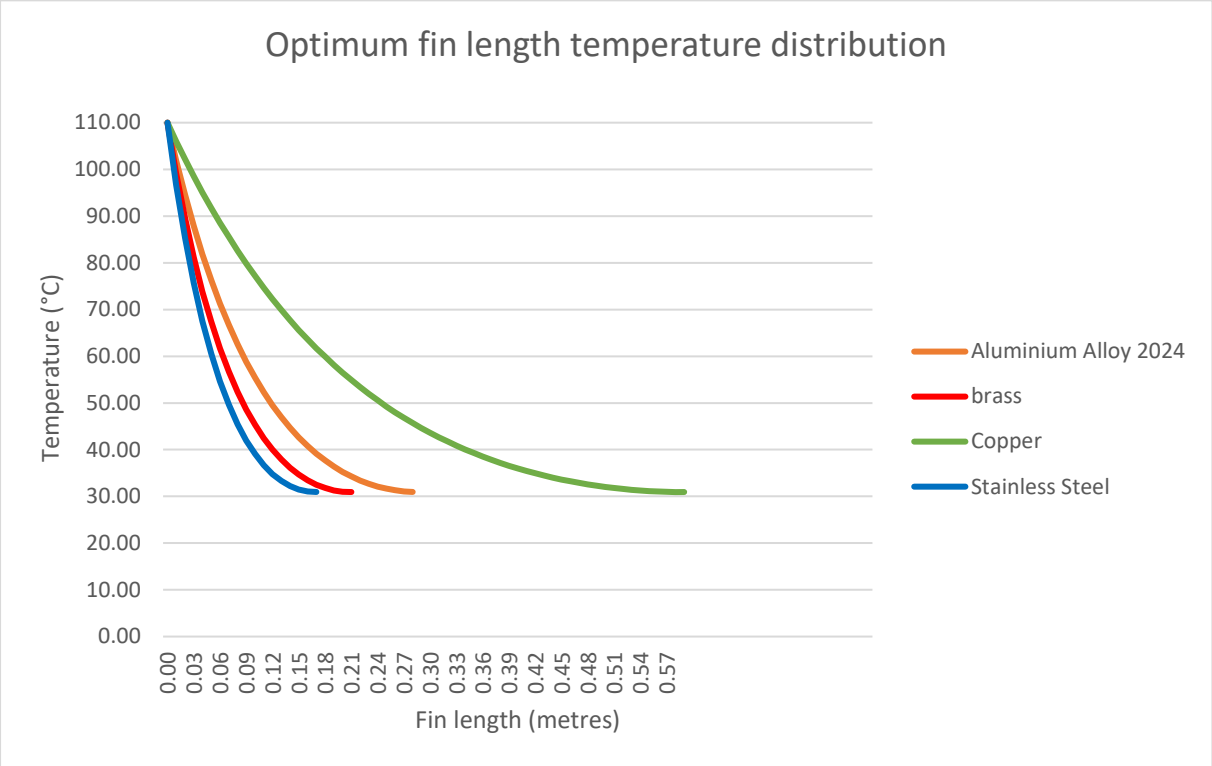

Figure 26-Plot showing the temperature distribution of the optimum length rods.

Material	Temperature distribution at optimum length (°C)
Aluminium	30.95
Brass	30.94
Copper	30.94
Stainless steel	30.94

Table 5-Temperature distribution at optimum lengths

3.2.5 Analysis of Temperature Distribution for Optimum Lengths

The calculation seen in Section 3.1.3 was repeated with modified values, using the mL criterion stated in Section 3.2 and calculated in Section 3.2.3, based on the optimum length parameters calculated in Section 3.2.1.

Fig. 24 illustrates the temperature decay along each rod with greater clarity. In comparison to the heat loss values of 3.1.8 and the results of 3.2.3, it is evident that the heat loss values for aluminium, brass, and stainless steel have decreased negligibly, while the length of the fin has decreased significantly. This suggests that lengths beyond the optimum would be a waste of material as the temperature has stabilised at around 30 °C. A further observation of the data shows that the temperature of these optimised lengths has increased from around 20 °C to 30 °C, which is above the ambient temperature and suggests optimal thermal conduction. Additionally, it indicates an inversely proportional relationship between mL and heat conduction. This is correlated with the results for copper, which was the only material which showed an increase in heat loss and a drop in temperature in comparison to the plot shown in 3.1.7, which can be attributed to the length increasing to 0.59m, thus increasing surface area(Incropera et al., 2007) and the mL increasing from 1.79 to 2.65.

3.3 Accurate Fin Length Prediction

As an infinite fin boundary condition(assuming heat flux at the tip) has been stipulated for predicting a more accurate fin length, calculating the temperature distribution in this case is expressed as(Lienhard, 2020) :

$$T(x) = T_\infty + (T_b - T_\infty) \cdot \tanh(mL)$$

Equation 7-Temperature distribution for an infinite tip fin.

3.3.1 Solving exponential equation for L

A more precise length is calculated by ensuring that the tip temperature must be almost equal to the ambient fluid temperature; it follows that a stricter convergence criterion must be used, shown as:

$$e^{-mL} < 0.02$$

Equation 8-Stricter convergence criteria.

To solve the exponential Eq.8 for L, natural logarithms are taken of both sides:

$$ln(e^{-mL}) < ln(0.02)$$

Resulting in:

$$-mL < ln(0.02)$$

The equation is rearranged to make L the subject gives:

$$L = \frac{ln(0.02)}{-m}$$

3.3.2 Calculating more accurate fin length

3.3.2.1 Aluminium alloy

$$L = \frac{ln(0.02)}{-9.2748}$$

$$L = 0.4218\ m$$

3.3.2.2 Brass

$$L = \frac{ln(0.02)}{-12.7128}$$

$$L = 0.3077\ m$$

3.3.2.3 Copper

$$L = \frac{ln(0.02)}{-4.4834}$$

$$L = 0.8726\ m$$

3.3.2.4 Stainless Steel

$$L = \frac{ln(0.02)}{-15.8114}$$

$$L = 0.2474\ m$$

3.3.3 Recalculated mL using stricter convergence criteria lengths

Material	mL	=
2024 Aluminium alloy	9.2748 X 0.4218	3.91
Brass (70 Cu/30 Zn)	12.7128 X 0.3077	3.91
Copper	4.4834 X 0.8726	3.91
304 Stainless Steel	15.8114 X 0.2474	3.91

Table 6-Recalculated mL values using the lengths calculated from stricter convergence criteria.

3.3.4Temperature Distribution Plot adjusted for stricter convergence criteria

The full data range is provided in App.3.

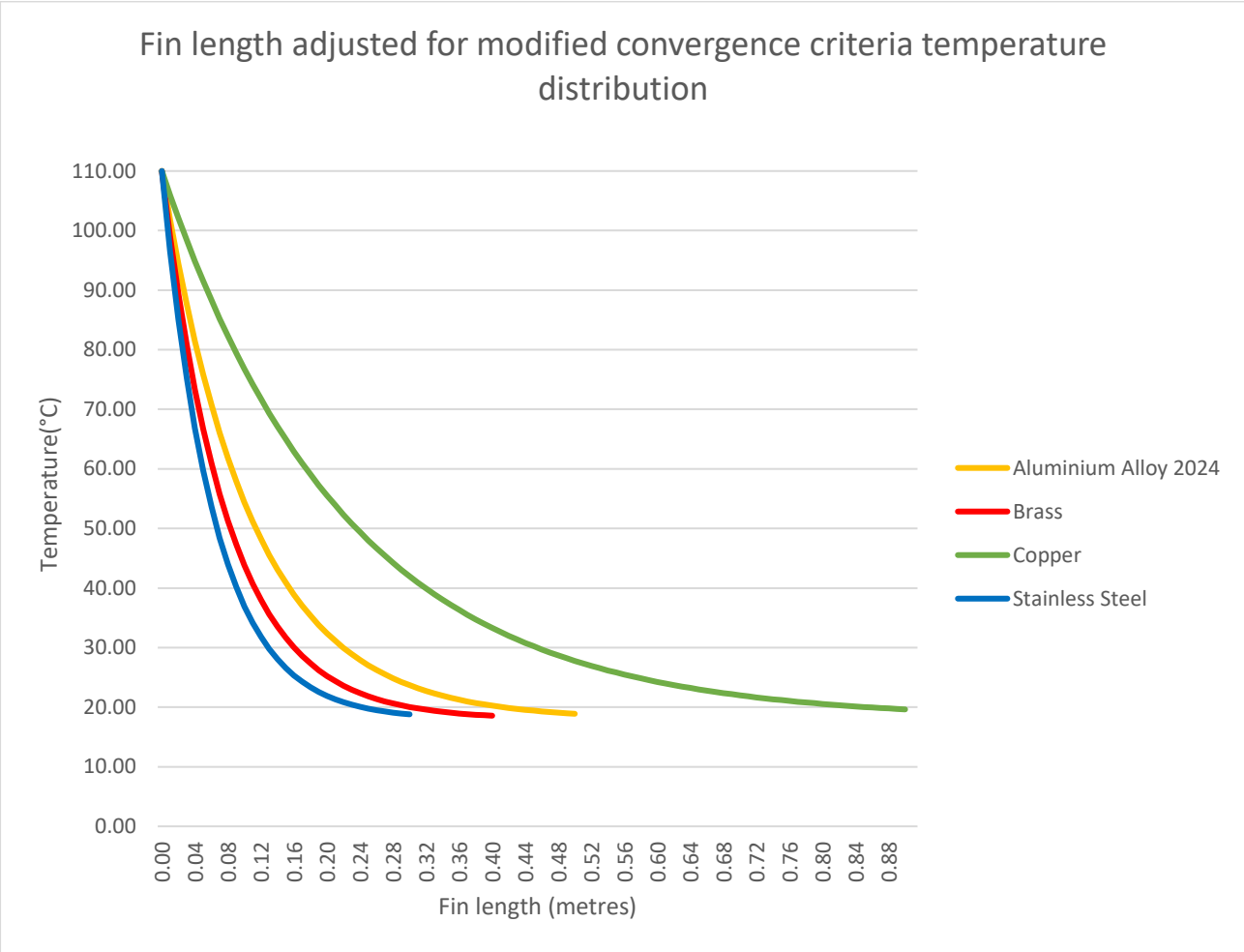

Figure 27-Plot showing the heat distribution of the four metal rods calculated from the stricter criterion.

Material	Temperature distribution at more accurate fin length(°C)
Aluminium	18.89
Brass	18.57
Copper	19.63
Stainless steel	18.80

Table 7-Temperature distribution at more accurate length

3.3.5 Heat transfer recalculation for stricter convergence criteria

Using the infinite fin approximation, assuming heat transfer at the tip expressed as:

$$\dot{Q} = \sqrt{hPkA_c}(T_b - T_\infty)$$

Equation 9-Rate of heat transfer for an infinite fin

Using Eq.9, the heat loss for the four rod lengths calculated in 3.3.2 are shown as:

3.3.5.1 Aluminium alloy

$$\dot{Q} = \sqrt{30 \times (0.236) \times 186 \times (0.0375)} \cdot (110 - 18)$$

$$\dot{Q} = 7.01\ W$$

3.3.5.2 Brass

$$\dot{Q} = \sqrt{30 \times (0.236) \times 99 \times (0.0375)} \cdot (110 - 18)$$

$$\dot{Q} = 5.11\ W$$

3.3.5.3 Copper

$$\dot{Q} = \sqrt{15 \times (0.236) \times 398 \times (0.0375)} \cdot (110 - 18)$$

$$\dot{Q} = 7.25\ W$$

3.3.5.4 Stainless Steel

$$\dot{Q} = \sqrt{7.5 \times (0.236) \times 16 \times (0.0375)} \cdot (110 - 18)$$

$$\dot{Q} = 1.03\ W$$

3.3.6 Analysis and comparison

We observe that enforcing the criteria outlined in 3.3.1 increases the fin length by approximately 30–50% beyond the optimum length for all materials. For aluminium, brass, and stainless steel, the 0.4 m rods shown in 3.1.5 were already longer than these optimised lengths; thus, those rods were more than sufficient to dissipate heat. In fact, for stainless steel and brass, 0.4 m was nearly double the optimum length, indicating that much of the rod provided no additional cooling as temperatures approached ambient levels well before the tip (as shown in Fig. 25 & Tab.2) (Lienhard, 2020). Aluminium's 0.4 m rod was also significantly longer than necessary.

Copper is the exception: its more accurate optimum length is 0.873 m, which is over twice the length used in section 3.1.1. At 0.873 m, the copper fin would dissipate 7.25 W, whereas the 0.4 m copper fin lost 6.86 W. This represents a 5.5% increase in heat transfer, even though it results in nearly doubling the rod's length. However, beyond 0.9 m, returns diminish rapidly – adding additional length would yield negligible extra heat loss(Incropera et al., 2007).

In summary, using the efficiency criterion shown in 4.2 is usually sufficient(Incropera et al., 2007) (Lienhard, 2020), as the more accurate criterion demonstrates only marginal improvements in heat loss while requiring significantly longer fins, underscoring the diminishing returns for very long fins(Incropera et al., 2007) (Kumar and Pandey, 2025).

References

1970 - 1972 Camaro Engine Cooling Clutch Fan Blade, GM 3976064 with Date Code E70 ([no date]). Available at: https://www.CAMAROCENTRAL.COM/product_p/rad-543.htm (Accessed: 30 March 2025).

Abrams, M. (2012) *Gottlieb Daimler*. Available at: https://www.asme.org/topics-resources/content/Gottlieb-Daimler (Accessed: 29 March 2025).

Amirpour, S., Orbay, R., Thiringer, T., Samani, M.K., Mademlis, G., Larsson, D. and Andersson, A. (2024) 'Highly thermal conductive graphene-based heatsink tailored for electric propulsion SiC-based inverter'. *Applied Thermal Engineering* 243, p. 122548. Available at: doi:10.1016/j.applthermaleng.2024.122548.

ANSYS FLUENT: CFD simulation for 3D radiator - YouTube (2022). Available at: https://www.youtube.com/watch?v=Jqa5ViPSE9M (Accessed: 30 March 2025).

Anthony, S. (2011) *Intel 4004, the first CPU, is 40 years old today*. Available at: https://www.extremetech.com/computing/105029-intel-4004-the-first-cpu-is-40-years-old-today (Accessed: 30 March 2025).

Aslan, Y., Puskely, J., Janssen, J.H.J., Geurts, M., Roederer, A. and Yarovoy, A. (2018) 'Thermal-Aware Synthesis of 5G Base Station Antenna Arrays: An Overview and a Sparsity-Based Approach'. *IEEE Access* 6, pp. 58868–58882. Available at: doi:10.1109/ACCESS.2018.2873977.

Baker, B. (2024) '10 horsepower BSA. RWDCar 1921 | The BSA Front Wheel Drive Club'. Available at: https://www.bsafwdc.org/magazine-articles-republished/554-2/ (Accessed: 29 March 2025).

Baknor Thermal Management, Heat Sinks, Liquid Cold Plates & More. (2025). Available at: https://www.baknorthermal.com/force-convection-fan-heat-sinks/ (Accessed: 30 March 2025).

Beatenbough, P.K. (1968) 'Engine Cooling Systems for Motor Trucks'. *SAE Transactions* 76, pp. 205–235.

Bird, J.O. (2021) *Bird's basic engineering mathematics*. Eighth edition. Abingdon, Oxon ; New York: Routledge.

Budimir, M. (2000) *Cooling the pin-fin way*. Available at: https://www.machinedesign.com/archive/article/21814903/cooling-the-pin-fin-way (Accessed: 30 March 2025).

Cermak, M., Kenna, J. and Bahrami, M. (2017) 'Natural-graphite-sheet based heat sinks'. in *2017 33rd Thermal Measurement, Modeling & Management Symposium (SEMI-THERM)*., pp. 310–313. Available at: doi:10.1109/SEMI-THERM.2017.7896947 (Accessed: 30 March 2025).

Chen, H., Zhang, T., Gao, Q., Lv, J., Chen, H. and Huang, H. (2025) 'Thermal management enhancement of electronic chips based on novel technologies'. *Energy* 316, p. 134575. Available at: doi:10.1016/j.energy.2025.134575.

Chen, K.-L., Luo, K.-Y., Gupta, P.P. and Kang, S.-W. (2023) 'SLM Additive Manufacturing of Oscillating Heat Pipe'. *Sustainability* 15(9), p. 7538. Available at: doi:10.3390/su15097538.

Cheung, M. (2020) 'The State of Microprocessor Cooling Systems'. *The Startup* 6 December. Available at: https://medium.com/swlh/the-state-of-microprocessor-cooling-systems-d26ae3876c1e (Accessed: 30 March 2025).

Chiou, J.P. (1975) 'Engine Cooling System of Military Combat/Tactical Vehicles'. *SAE Transactions* 84, pp. 173–191.

Dede, E.M. (2014) 'Single-phase microchannel cold plate for hybrid vehicle electronics'. in *2014 Semiconductor Thermal Measurement and Management Symposium (SEMI-THERM)*., pp. 118–124. Available at: doi:10.1109/SEMI-THERM.2014.6892227 (Accessed: 29 March 2025).

Diamant, N.S. (1924) 'Engine-Cooling Systems and Radiator Characteristics'. *SAE Transactions* 19, pp. 295–336.

Do Electric Vehicles Have Radiators? - CHAL (2024). Available at: https://www.chaluminium.com/do-electric-vehicles-have-radiators (Accessed: 30 March 2025).

Farzanehnia, A., Khatibi, M., Sardarabadi, M. and Passandideh-Fard, M. (2019) 'Experimental investigation of multiwall carbon nanotube/paraffin based heat sink for electronic device thermal management'. *Energy Conversion and Management* 179, pp. 314–325. Available at: doi:10.1016/j.enconman.2018.10.037.

finskiving.com (2025). Available at: https://www.finskiving.com/in-need-of-a-skived-heatsink (Accessed: 30 March 2025).

Flat Tube and Fin Radiator Cores ([no date]). Available at: https://www.thebrassworks.net/products/flat-tube-and-fin-radiator-cores (Accessed: 30 March 2025).

Fortin, P.E., Kellermann, W.M., Smith, F.N., Rogers, C.J. and Wheeler, M.J. (1985) 'Aluminum Materials and Processes for Automotive Heat Exchanger Applications'. *SAE Transactions* 94, pp. 1020–1031.

Furber, S. (2017) 'Microprocessors: the engines of the digital age'. *Proceedings: Mathematical, Physical and Engineering Sciences* 473(2199), pp. 1–12.

Gulhame, A. (2015) *(PDF) EXPERIMENTAL INVESTIGATION OF CONVECTIVE HEAT TRANSFER FOR RADIATOR BY USING NANOFLUID*. Available at: doi:10.13140/RG.2.2.20241.84320 (Accessed: 30 March 2025).

Guo, Y., Yang, H., Lin, G., Jin, H., Shen, X., He, J. and Miao, J. (2021) 'Thermal performance of a 3D printed lattice-structure heat sink packaging phase change material'. *Chinese Journal of Aeronautics* 34(5), pp. 373–385. Available at: doi:10.1016/j.cja.2020.07.033.

Hirasawa, T., Kawabata, K. and Oomi, M. (2005) 'Evolution of the Heatsink Technology'.

'Honeycomb' radiator ([no date]). Available at: https://mercedes-benz-publicarchive.com/marsClassic/en/instance/picture/Honeycomb-radiator.xhtml?oid=122213 (Accessed: 30 March 2025).

Hoyt, G.W. (1919) 'Radiator Cooling Fans'. *SAE Transactions* 14, pp. 758–776.

Hyun, L.K. and Pil, W.J. (1996) 'Thermal Design of Compact Circular External Water Cooled Engine Oil Cooler'. *SAE Transactions* 105, pp. 1660–1668.

Incropera, F.P., DeWitt, D.P., Bergman, T.L. and Lavine, A.S. (eds.) (2007) *Fundamentals of heat and mass transfer*. 6. ed. Hoboken, NJ: Wiley.

Katsutani, H., Yamagata, S. and Nakamura, I. (2016) 'History and Future Development of Heat Spreader Products'.

Kumar, R. and Pandey, M. (2025) 'Numerical analysis of heat transfer and fluid flow characteristics of microchannel heat sinks with streamwise variation of fin height'. *International Communications in Heat and Mass Transfer* 163, p. 108706. Available at: doi:10.1016/j.icheatmasstransfer.2025.108706.

Lawrence, C. (1922) 'Air cooled engine development'. *SAE Transactions* 17(1), pp. 431–477.

Leslie, S.W. (1979) 'Charles F. Kettering and the Copper-Cooled Engine'. *Technology and Culture* 20(4), pp. 752–776. Available at: doi:10.2307/3103638.

Li, Y., Eldredge, J.D., Lavine, A.S., Fisher, T.S. and Drolen, B.L. (2024) 'A conjugate heat transfer model of oscillating heat pipe dynamics, performance, and dryout'. *International Journal of Heat and Mass Transfer* 227, p. 125530. Available at: doi:10.1016/j.ijheatmasstransfer.2024.125530.

Lienhard, J.H. (2020) *A heat transfer textbook*. Fifth edition. New York: Dover Publications.

'Litchfield Toyota GR Yaris Intercooler with Engine Oil Cooler | Litchfield Motors'. (2025). Available at: https://www.litchfieldmotors.com/shop/toyota/gr-yaris/hatchback-xp210-2020/1-6-turbo/cooling-1-6-turbo/litchfield-toyota-gr-yaris-intercooler-with-engine-oil-cooler/ (Accessed: 30 March 2025).

MCG (2022) 'The 1923 Copper-Cooled Chevrolet: What Went Wrong?'. *Mac's Motor City Garage* 8 March. Available at: https://www.macsmotorcitygarage.com/the-1923-copper-cooled-chevrolet-what-went-wrong/ (Accessed: 29 March 2025).

Mochizuki, M., Nguyen, T., Mashiko, K., Saito, Y., Nguyen, T. and Wuttijumnong, V. (2011) 'A REVIEW OF HEAT PIPE APPLICATION INCLUDING NEW OPPORTUNITIES'. *Frontiers in Heat Pipes* 2(1). Available at: doi:10.5098/fhp.v2.1.3001 (Accessed: 30 March 2025).

Mohamed, K.A., Younis, O. and Hussein, A.K. (2019) 'Numerical Investigation Of Possibility Of Using Shape Memory Alloy In Louvered Fins Radiators'. 11(3)

Newcomb, T.P., Spurr, R.T., Newcomb, T.P. and Spurr, R.T. (1989) *A technical history of the motor car*. Bristol: Hilger.

Nicol, C. (2024) 'GMG's THERMAL-XR® Demonstrates Potential for Electronics Heat Sink Miniaturization and Efficiency'. *Graphene Manufacturing Group | GMG* 11 December. Available at: https://graphenemg.com/gmgs-thermal-xr-demonstrates-potential-for-electronics-heat-sink-miniaturization-and-efficiency/ (Accessed: 30 March 2025).

Noda, H., Ikeda, M., Kimura, Y. and Kawabata, K. (2005) 'Development of High-Performance Heatsink "Crimped fin®"'.

Piao, C., Chen, T., Zhou, A., Wang, P. and Chen, J. (2020) 'Research on Electric Vehicle Cooling System Based on Active and Passive Liquid Cooling'. *Journal of Physics: Conference Series* 1549(4), p. 042146. Available at: doi:10.1088/1742-6596/1549/4/042146.

Pongiannan, S., Ramalingam, V. and Nagendran, L. (2019) 'Natural-convection heat transfer enhancement of aluminum heat sink using nanocoating by electron beam method'. *Thermal Science* 23(5 Part B), pp. 3129–3141. Available at: doi:10.2298/TSCI170830007P.

Radiator cooling for car | 3D CAD Model Library | GrabCAD (2025). Available at: https://grabcad.com/library/radiator-cooling-for-car-1 (Accessed: 30 March 2025).

Ramesh Kumar, R., Karthik, K., Elumalai, P.V., Elumalai, R., Chandran, D., Prakash, E. and Hassin, N. (2024) 'Enhancing automotive cooling systems: composite fins and nanoparticles analysis in radiators'. *Scientific Reports* 14(1), p. 3650. Available at: doi:10.1038/s41598-024-52141-0.

Reyes, M., Alonso, D., Arias, J.R. and Velazquez, A. (2012) 'Experimental and theoretical study of a vapour chamber based heat spreader for avionics applications'. *Applied Thermal Engineering* 37, pp. 51–59. Available at: doi:10.1016/j.applthermaleng.2011.12.050.

Saunders, L.P. (1936) 'Radiator Development and Car Cooling'. *SAE Transactions* 31, pp. 496–516.

Shah, R.K. (2003) 'Advances in Automotive Heat Exchanger Technology'. *SAE Transactions* 112, pp. 631–641.

Shariff, K., Abdullahi, B. and Abubakar, S.B. (2018) 'Modelling and Simulation of Car Radiator : Effects of Fins under the Atmospheric Condition of Kano , Nigeria'. Available at: https://www.semanticscholar.org/paper/Modelling-and-Simulation-of-Car-Radiator-%3A-Effects-Shariff-Abdullahi/d6bf7e51cb77f3e29efc1bad6f915bbd160ef78c (Accessed: 29 March 2025).

Shibata, Y., Hosaka, S., Fujitani, K. and Himeno, R. (1990) 'A Numerical Analysis Method for Optimizing Intercooler Design in the Vehicle Development Process'. *SAE Transactions* 99, pp. 402–414.

SIGRATHERM (2025). Available at: https://www.sglcarbon.com/en/markets-solutions/applications/thermal-management/ (Accessed: 30 March 2025).

Suffri Shamsuddin, H., Wei Tong, L., Mohd-Ghazali, N., Estellé, P., Maré, T. and Mohamad, M. (2021) 'Nanofluid-Cooled Microchannel Heat Sink with Carbon Nanotube'. *EVERGREEN Joint Journal of Novel Carbon Resource Sciences & Green Asia Strategy* 08(01), pp. 170–176.

Volkswagen (2003) *The Volkswagen Beetle, a success story*. Available at: https://www.volkswagen-newsroom.com/en/the-volkswagen-beetle-a-success-story-2341.

Westcott, J.H. (1979) 'Review Lecture: The Application of Microprocessors'. *Proceedings of the Royal Society of London. Series A, Mathematical and Physical Sciences* 367(1731), pp. 451–484.

Appendices

Appendix 1

Al		Brass		Copper		Stainless Steel	
Distance values at x	Temp distribution	Distance values a	Temp distribution	Distance values at x	Temp distribution	Distance valu	Temp distribution
0.00	110.00	0.00	110.00	0.00	110.00	0.00	110.00
0.01	101.86	0.01	99.02	0.01	106.19	0.01	96.55
0.02	94.44	0.02	89.35	0.02	102.55	0.02	85.06
0.03	87.69	0.03	80.83	0.03	99.09	0.03	75.25
0.04	81.53	0.04	73.33	0.04	95.79	0.04	66.88
0.05	75.91	0.05	66.73	0.05	92.65	0.05	59.73
0.06	70.80	0.06	60.91	0.06	89.65	0.06	53.63
0.07	66.14	0.07	55.79	0.07	86.80	0.07	48.42
0.08	61.90	0.08	51.28	0.08	84.09	0.08	43.97
0.09	58.03	0.09	47.31	0.09	81.51	0.09	40.17
0.10	54.51	0.10	43.81	0.10	79.06	0.10	36.93
0.11	51.30	0.11	40.74	0.11	76.73	0.11	34.16
0.12	48.38	0.12	38.03	0.12	74.52	0.12	31.80
0.13	45.72	0.13	35.64	0.13	72.42	0.13	29.78
0.14	43.30	0.14	33.54	0.14	70.43	0.14	28.06
0.15	41.09	0.15	31.69	0.15	68.55	0.15	26.59
0.16	39.09	0.16	30.06	0.16	66.77	0.16	25.33
0.17	37.27	0.17	28.63	0.17	65.09	0.17	24.26
0.18	35.61	0.18	27.37	0.18	63.50	0.18	23.35
0.19	34.10	0.19	26.26	0.19	62.00	0.19	22.57
0.20	32.74	0.20	25.28	0.20	60.59	0.20	21.90
0.21	31.50	0.21	24.42	0.21	59.27	0.21	21.33
0.22	30.37	0.22	23.67	0.22	58.03	0.22	20.85
0.23	29.36	0.23	23.01	0.23	56.87	0.23	20.43
0.24	28.44	0.24	22.43	0.24	55.79	0.24	20.08
0.25	27.61	0.25	21.92	0.25	54.79	0.25	19.78
0.26	26.86	0.26	21.47	0.26	53.86	0.26	19.53
0.27	26.19	0.27	21.08	0.27	53.00	0.27	19.31
0.28	25.59	0.28	20.74	0.28	52.21	0.28	19.12
0.29	25.05	0.29	20.45	0.29	51.49	0.29	18.97
0.30	24.58	0.30	20.19	0.30	50.84	0.30	18.84
0.31	24.16	0.31	19.97	0.31	50.25	0.31	18.72
0.32	23.80	0.32	19.78	0.32	49.73	0.32	18.63
0.33	23.48	0.33	19.62	0.33	49.27	0.33	18.55
0.34	23.22	0.34	19.49	0.34	48.88	0.34	18.49
0.35	22.99	0.35	19.38	0.35	48.54	0.35	18.44
0.36	22.81	0.36	19.29	0.36	48.27	0.36	18.40
0.37	22.68	0.37	19.22	0.37	48.06	0.37	18.37
0.38	22.58	0.38	19.18	0.38	47.91	0.38	18.35
0.39	22.52	0.39	19.15	0.39	47.82	0.39	18.33
0.40	22.50	0.40	19.14	0.40	47.79	0.40	18.33

Appendix 2

Aluminium Alloy 2024		brass		Copper		Stainless Steel	
Distance values (x)	Optimum length temp distrubution	Distance va	Optimum length temp distrubution	Distance value	Optimum length temp distrubution	Distance valu	Optimum length temp distrubution
0.00	110.00	0.00	110.00	0.00	110.00	0.00	110.00
0.01	101.94	0.01	99.13	0.01	106.01	0.01	96.69
0.02	94.59	0.02	89.58	0.02	102.19	0.02	85.35
0.03	87.91	0.03	81.19	0.03	98.55	0.03	75.70
0.04	81.83	0.04	73.81	0.04	95.06	0.04	67.50
0.05	76.30	0.05	67.34	0.05	91.73	0.05	60.53
0.06	71.27	0.06	61.67	0.06	88.55	0.06	54.63
0.07	66.70	0.07	56.71	0.07	85.51	0.07	49.65
0.08	62.55	0.08	52.37	0.08	82.61	0.08	45.46
0.09	58.78	0.09	48.59	0.09	79.83	0.09	41.96
0.10	55.37	0.10	45.30	0.10	77.18	0.10	39.06
0.11	52.27	0.11	42.46	0.11	74.65	0.11	36.68
0.12	49.47	0.12	40.01	0.12	72.24	0.12	34.78
0.13	46.94	0.13	37.92	0.13	69.93	0.13	33.29
0.14	44.66	0.14	36.15	0.14	67.72	0.14	32.19
0.15	42.61	0.15	34.67	0.15	65.62	0.15	31.44
0.16	40.77	0.16	33.47	0.16	63.61	0.16	31.03
0.17	39.13	0.17	32.51	0.17	61.70	0.17	30.94
0.18	37.67	0.18	31.79	0.18	59.87		
0.19	36.38	0.19	31.29	0.19	58.13		
0.20	35.24	0.20	31.01	0.20	56.46		
0.21	34.26	0.21	30.94	0.21	54.88		
0.22	33.41			0.22	53.37		
0.23	32.70			0.23	51.92		
0.24	32.12			0.24	50.55		
0.25	31.65			0.25	49.25		
0.26	31.31			0.26	48.00		
0.27	31.07			0.27	46.82		
0.28	30.95			0.28	45.69		
				0.29	44.62		
				0.30	43.60		
				0.31	42.64		
				0.32	41.72		
				0.33	40.86		
				0.34	40.03		
				0.35	39.26		
				0.36	38.52		
				0.37	37.83		
				0.38	37.17		
				0.39	36.56		
				0.40	35.98		
				0.41	35.44		
				0.42	34.93		
				0.43	34.46		
				0.44	34.02		
				0.45	33.61		
				0.46	33.23		
				0.47	32.89		
				0.48	32.57		
				0.49	32.29		
				0.50	32.03		
				0.51	31.80		
				0.52	31.60		
				0.53	31.42		
				0.54	31.28		
				0.55	31.16		
				0.56	31.06		
				0.57	30.99		
				0.58	30.95		
				0.59	30.94		

Appendix 3

Aluminium Alloy 2024		Brass		Copper		Stainless Steel	
Length of fin	Temp distribution	Length of fin	Temp distribution	Length of fin	Temp distribution	Length of fin	Temp distribution
0.00	110.00	0.00	110.00	0.00	110.00	0.00	110.00
0.01	101.85	0.01	99.02	0.01	105.97	0.01	96.55
0.02	94.42	0.02	89.35	0.02	102.11	0.02	85.06
0.03	87.65	0.03	80.83	0.03	98.42	0.03	75.25
0.04	81.48	0.04	73.33	0.04	94.90	0.04	66.88
0.05	75.86	0.05	66.72	0.05	91.52	0.05	59.73
0.06	70.74	0.06	60.91	0.06	88.30	0.06	53.63
0.07	66.06	0.07	55.78	0.07	85.22	0.07	48.42
0.08	61.81	0.08	51.27	0.08	82.27	0.08	43.97
0.09	57.93	0.09	47.30	0.09	79.45	0.09	40.17
0.10	54.39	0.10	43.80	0.10	76.76	0.10	36.93
0.11	51.17	0.11	40.72	0.11	74.18	0.11	34.16
0.12	48.23	0.12	38.01	0.12	71.72	0.12	31.80
0.13	45.55	0.13	35.62	0.13	69.36	0.13	29.78
0.14	43.11	0.14	33.52	0.14	67.11	0.14	28.06
0.15	40.89	0.15	31.67	0.15	64.96	0.15	26.59
0.16	38.86	0.16	30.03	0.16	62.90	0.16	25.33
0.17	37.01	0.17	28.60	0.17	60.93	0.17	24.26
0.18	35.33	0.18	27.33	0.18	59.05	0.18	23.34
0.19	33.79	0.19	26.22	0.19	57.25	0.19	22.56
0.20	32.39	0.20	25.24	0.20	55.53	0.20	21.89
0.21	31.12	0.21	24.37	0.21	53.88	0.21	21.32
0.22	29.96	0.22	23.61	0.22	52.31	0.22	20.84
0.23	28.90	0.23	22.94	0.23	50.81	0.23	20.42
0.24	27.93	0.24	22.35	0.24	49.37	0.24	20.07
0.25	27.05	0.25	21.83	0.25	47.99	0.25	19.77
0.26	26.25	0.26	21.38	0.26	46.68	0.26	19.51
0.27	25.52	0.27	20.97	0.27	45.42	0.27	19.29
0.28	24.85	0.28	20.62	0.28	44.22	0.28	19.10
0.29	24.25	0.29	20.30	0.29	43.07	0.29	18.94
0.30	23.69	0.30	20.03	0.30	41.97	0.30	18.80
0.31	23.19	0.31	19.79	0.31	40.92		
0.32	22.73	0.32	19.57	0.32	39.91		
0.33	22.31	0.33	19.39	0.33	38.95		
0.34	21.93	0.34	19.22	0.34	38.03		
0.35	21.58	0.35	19.07	0.35	37.16		
0.36	21.26	0.36	18.95	0.36	36.32		
0.37	20.97	0.37	18.83	0.37	35.51		
0.38	20.71	0.38	18.73	0.38	34.75		
0.39	20.47	0.39	18.65	0.39	34.01		
0.40	20.25	0.40	18.57	0.40	33.31		
0.41	20.05			0.41	32.64		
0.42	19.87			0.42	32.00		
0.43	19.71			0.43	31.38		
0.44	19.55			0.44	30.80		
0.45	19.42			0.45	30.23		
0.46	19.29			0.46	29.70		
0.47	19.18			0.47	29.19		
0.48	19.07			0.48	28.70		
0.49	18.98			0.49	28.23		
0.50	18.89			0.50	27.78		

				0.51	27.35		
				0.52	26.94		
				0.53	26.55		
				0.54	26.17		
				0.55	25.81		
				0.56	25.47		
				0.57	25.14		
				0.58	24.83		
				0.59	24.53		
				0.60	24.24		
				0.61	23.97		
				0.62	23.71		
				0.63	23.46		
				0.64	23.22		
				0.65	22.99		
				0.66	22.77		
				0.67	22.56		
				0.68	22.36		
				0.69	22.17		
				0.70	21.99		
				0.71	21.81		
				0.72	21.65		
				0.73	21.49		
				0.74	21.33		
				0.75	21.19		
				0.76	21.05		
				0.77	20.91		
				0.78	20.79		
				0.79	20.66		
				0.80	20.55		
				0.81	20.44		
				0.82	20.33		
				0.83	20.23		
				0.84	20.13		
				0.85	20.04		
				0.86	19.95		
				0.87	19.86		
				0.88	19.78		
				0.89	19.70		
				0.90	19.63		